

Chapter 5

Results

In this chapter predicted properties of intrinsic defects and defects due to fission product accommodation in UO_2 and U_3O_8 are presented. The results were obtained using atomistic simulation techniques based on energy minimisation as described in Chapter 2. In the first section, intrinsic defects and fission products in UO_2 are discussed. The second section deals with U_3O_8 . Where experimental data are available, these are compared with the results.

5.1 UO_2

5.1.1 Inter-ionic Potentials

The first part of this subsection concerns intrinsic defects. Two potentials are used to simulate the properties of the UO_2 lattice. Table 5.1 shows the short range interaction parameters used in this study.

The first set of inter-ionic potentials (Potential I) is based on work by Catlow and Grimes [100] and were used to study the solution behaviour of fission products

	Potential I	Potential II	Unit
Buckingham potentials:			
O – O	$A = 108.0$	$A = 9547.96$	eV
	$\rho = 0.38$	$\rho = 0.2192$	Å
	$C = 56.06$	$C = 32$	eVÅ ⁶
U ⁴⁺ – O	$A = 2494.2$	$A = 1761.775$	eV
	$\rho = 0.34123$	$\rho = 0.356421$	Å
	$C = 40.16$	$C = 0$	eVÅ ⁶
U ⁴⁺ – U ⁴⁺	$A = 18600.0$	$A = 0$	eV
	$\rho = 0.27468$		Å
	$C = 32.64$		eVÅ ⁶
U ⁵⁺ – U ⁴⁺	$A = 3089.54$	$A = 1868.5$	eV
	$\rho = 0.33226$	$\rho = 0.35942$	Å
	$C = 50.56$	$C = 0$	eVÅ ⁶
Shell parameters:			
O	$Y = -4.4$	$Y = -2.04$	e
	$k = 296.8$	$k = 6.3$	eVÅ ⁻²
U ⁴⁺	$Y = 6.54$	$Y = -0.1$	e
	$k = 98.24$	$k = 160.0$	eVÅ ⁻²
U ⁵⁺	$Y = 7.54$	$Y = 0$	e
	$k = 98.24$		eVÅ ⁻²

Table 5.1: The uranium and oxygen potential parameters used in this study. The parameters A , ρ and C are the parameters of the Buckingham potential form (equation 2.51). The shell parameters Y and k are the ion shell charge and the harmonic constant of the interaction between core and shell respectively (see equation 2.54).

in UO_2 . The potentials, derived from electron gas calculations were modified to fit the lattice parameter, the elastic modulus or the dielectric constant where these properties were available.

Since it is now understood that in order to achieve more accurate simulations it is important to derive self consistent sets of potentials, a uranium potential set based on the oxygen-oxygen interaction by Grimes *et al.* [101] has been derived and used to compare the intrinsic defect properties. This potential set is referred to as potential set II. This potential set is based on the same oxygen-oxygen interaction used in Chapter 6 of this thesis.

For the simulation of fission product behaviour later on in this chapter only ionic potentials based on the first set have been used.

5.1.2 Fission product potentials

The fission product potentials used in the study of the UO_2 lattice are listed in Table 5.2. Potentials for caesium and iodine were taken from a study by Grimes and Catlow [100] which focussed on the solution behaviour of fission product ions in $\text{UO}_{2\pm x}$. These potentials were again based on electron gas calculations and empirical fitting procedures.

Ruthenium

A set of potentials for ruthenium was added using the same methods as employed for the derivation of the original set. The Ru^{4+} potentials were also fitted to the RuO_2 structure. In nature, RuO_2 adopts the cassiterite or tin-oxide structure (Wyckoff: IV,ba [102]). The ionic arrangement is based on the $\text{D}_{4h}14$ (P4/mnm) structure with positions $2a$ and $4f$ occupied by ruthenium and oxygen ions respectively. The

predicted lattice parameters, $a = 4.45 \text{ \AA}$ and $b = 3.16 \text{ \AA}$, are close to the experimental values $a = 4.51 \text{ \AA}$ and $b = 3.11 \text{ \AA}$. However, the central force potentials do not reproduce the tetragonality of the cell very accurately. The predicted a/b ratio is 1.41 compared with an experimental value of 1.45. Using the Ru^{4+} potentials in Table 5.2, the lattice volume is predicted to be 62.6 \AA^3 compared with an experimental value of $63.3 \pm 0.3 \text{ \AA}^3$.

5.1.3 Ionization potentials

Since we will be investigating charge transfer reactions, it is important to know the ionization potentials of the ions considered in this study. The potentials listed in Table 5.3 were either taken from the CRC handbook [103] or in the case of ruthenium, calculated using DMol [104], as an experimental value for the Ru^{4+} ionization potential was not available. Comparison of experimental values with those predicted by quantum mechanical techniques is difficult since the inaccuracy of the measured values is not known.

UO ₂ Buckingham short-range potentials used in this study			
Atoms	A [eV]	ρ [Å]	C [eV Å]
Cs ⁺ — U ⁺⁴	18659.60	0.29505	48.62
Cs ⁺ — O ⁻²	649.60	0.41421	64.34
I ⁻ — U ⁺⁴	6366.08	0.33893	96.48
I ⁻ — O ⁻²	619.04	0.42657	114.23
I — U ⁺⁴	7948.45	0.31427	71.84
I — O ⁻²	465.13	0.44074	108.38
I ⁺ — U ⁺⁴	6275.23	0.32892	48.62
I ⁺ — O ⁻²	783.99	0.40252	64.34
I ⁺² — U ⁺⁴	7564.98	0.30910	42.58
I ⁺² — O ⁻²	1291.87	0.36808	41.61
Ru ⁰ — U ⁺⁴	1573.533	0.44653	0.0
Ru ⁰ — O ⁻²	3173.559	0.26770	0.0
Ru ⁺ — U ⁺⁴	2851.201	0.37310	0.0
Ru ⁺ — O ⁻²	2603.295	0.29410	0.0
Ru ⁺² — U ⁺⁴	6121.457	0.31310	0.0
Ru ⁺² — O ⁻²	2649.294	0.30238	0.0
Ru ⁺³ — U ⁺⁴	11117.430	0.27846	0.0
Ru ⁺³ — O ⁻²	2988.577	0.29821	0.0
Ru ⁺⁴ — U ⁺⁴	17717.22	0.25595	0.0
Ru ⁺⁴ — O ⁻²	3080.004	0.29072	0.0

Table 5.2: UO₂ fission product potentials used in this study. The caesium and iodine interactions are taken from Grimes 1991 [100]. The ruthenium potentials were derived for the presented work (see section 5.1.2).

Ionization potentials used in this study in eV.				
Ion	1st	2nd	3rd	4th
Ru Experimental [103]	7.37	16.76	28.47	
Ru Calculated	6.60	17.36	29.76	47.96
I ⁻ Experimental [103]	3.06	13.51	22.19	36

Table 5.3: This table shows the ionization potentials used in this study. The potentials for ruthenium were calculated as well as taken from literature (see text).

5.1.4 Perfect lattice results

The basic lattice properties of $\text{UO}_{2\pm x}$ were predicted using the “CASCADE” code. Lattice parameter, formation energy, dielectric properties and intrinsic defect properties are listed and compared with literature results in Table 5.4. Since the potentials were derived using the lattice parameter as a critical constant, the prediction for that property is exact. The lattice energy predicted here is 1-2 eV lower than the value derived from a Born-Haber cycle by Benson *et al.* [59].

The high frequency dielectric constant ϵ_∞ compares well with the experimental results. The high frequency property is easier to reproduce accurately because it depends critically on the choice of parameters for the core-shell model (See section 2.5). The static dielectric constant ϵ_0 is more difficult to fit as it depends on properties which are not in the model (e.g. interaction of electron states) and on the arrangement of the ions. Potential II seems to predict ϵ_0 more accurately than Potential I.

The predicted Schottky and Frenkel enthalpies are much higher than the experimental values.

5.1.5 Intrinsic defects in UO_2

The availability of intrinsic defects in UO_2 is an important parameter in defect reactions. The Frenkel reaction in particular compensates the stoichiometry changes in UO_2 :



What this means is that in $\text{UO}_{2\pm x}$ the concentration of the majority oxygen defect (i. e. $V_O^{\bullet\bullet}$ in UO_{2-x} but O_i'' in UO_{2+x}) is a function of x , whereas the other

Predicted properties of $\text{UO}_{2\pm x}$ compared with experimental results			
Property	Potential I	Potential II	Experimental value
<u>lattice</u>			
a	2.734 Å	2.734 Å	2.734 Å
H_L	-105.562 eV	-104.468 eV	-106.7 eV [59]
<u>dielectric properties</u> $[\epsilon_r]$			
ϵ_0	13.26	18.22	24
ϵ_∞	5.26	5.70	5.30
<u>elastic constants</u> $[10^9 \text{ Nm}^{-2}]$			
C_{11}	523.7	531.8	396 [54]
C_{12}	146.1	121.9	121 [54]
C_{44}	88.6	120.6	61 [54]
<u>intrinsic defects</u>			
E_S	13.23 eV	10.62 eV	6.0-7.0 eV
E_F	6.77 eV	6.35 eV	3.0-4.0 eV

Table 5.4: UO_2 crystal properties, predicted using potential set I and II compared with experimental values.

oxygen defect has a concentration of approximately $x \exp(\Delta H_{\text{Frenkel}}/k_B T)$.

The creation of uranium vacancies is controlled by the Schottky equilibrium:



The predicted Schottky reaction (5.2) yields a negative enthalpy when it is applied to the situation in UO_{2+x} :



Since the number of available sites within the unit cell are the same for V_U and O_i , mass action considerations predict that:

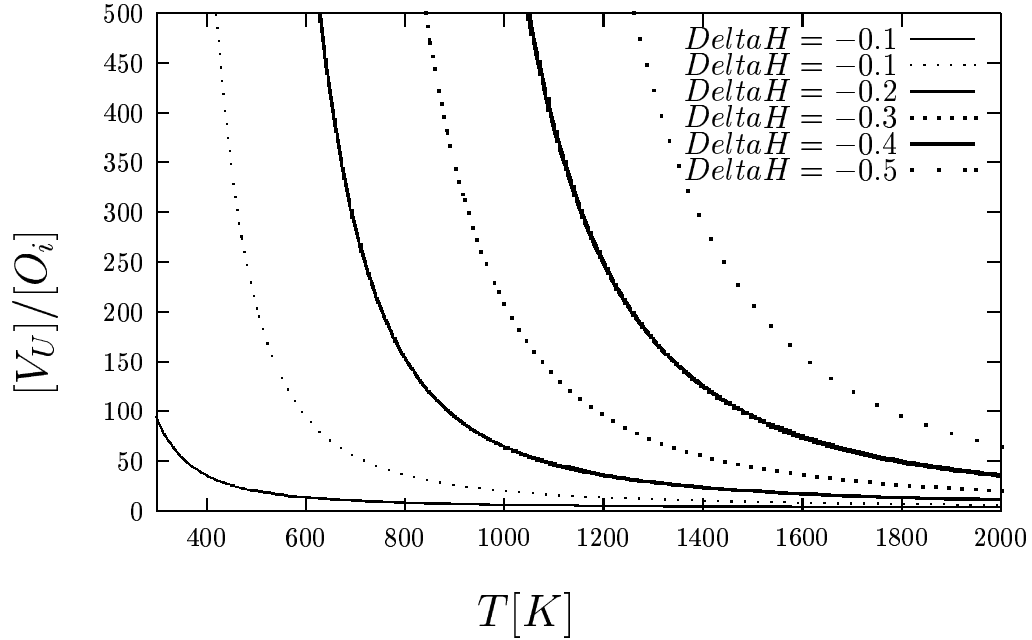
$$\frac{[V_U''']}{[O_i'']^2} = \exp\left(\frac{-\Delta H_S}{k_B T}\right). \quad (5.4)$$

Increasing temperatures will raise $[O_i'']$ relative to $[V_U''']$. The relative concentrations of $[U_V''']$ and $[O_i'']$ depend critically on the Schottky equilibrium enthalpy in UO_{2+x} , although the low temperature behaviour is probably not technologically important as the equilibrium situation portrayed by Figure 5.1 is only reached at elevated temperatures where defects are be mobile and where fuel operates.

Literature suggests that in UO_{2+x} oxygen interstitials are dominant over uranium vacancies and so ΔH_S must be positive. Neither of our potentials predict this. What is the effect of ΔH_S on the anion interstitial concentration in UO_{2+x} ?

x is equal to $[O_i] + 2[V_U]$. Substitution of equation 5.4 leads to a quadratic which can be approximated by:

$$[O_i''] = \begin{cases} \sqrt{x/2} \exp\left(\frac{\Delta H_S}{2k_B T}\right) & \text{if } \Delta H_S < 0, \\ x & \text{if } \Delta H_S > 0 \end{cases}. \quad (5.5)$$

Figure 5.1: Relative concentration of $[V_U]/[O_i]$.

The D_0 value in the diffusion equation will depend on the value of $[O_i'']$ and thus ΔH_S :

$$D_{O_i} = \begin{cases} \nu d^2 \sqrt{x/2} \exp\left(\frac{1/2\Delta H_S - \Delta H_M}{kT}\right), & \text{if } \Delta H_S < 0, \\ \nu d^2 x \exp\left(\frac{-\Delta H_M}{kT}\right), & \text{if } \Delta H_S > 0, \end{cases} \quad (5.6)$$

where ν is the attempt frequency.

Is ΔH_S really negative? One way to investigate this is to compare equations 5.6 with experimental evidence. Work by Contamin *et al.* [62] and Murch *et al.* [63] investigates the oxygen migration in UO_{2+x} as a function of stoichiometry. Figure 5.2 shows D_0 as a function of stoichiometry. The pre-exponentials in Figure 5.2 were determined at temperatures and stoichiometry compositions where, according to the phase diagram in Figure 4.1, no U_4O_9 is present.

For which case does Equation 5.6 fit Figure 5.2? Even though the data in

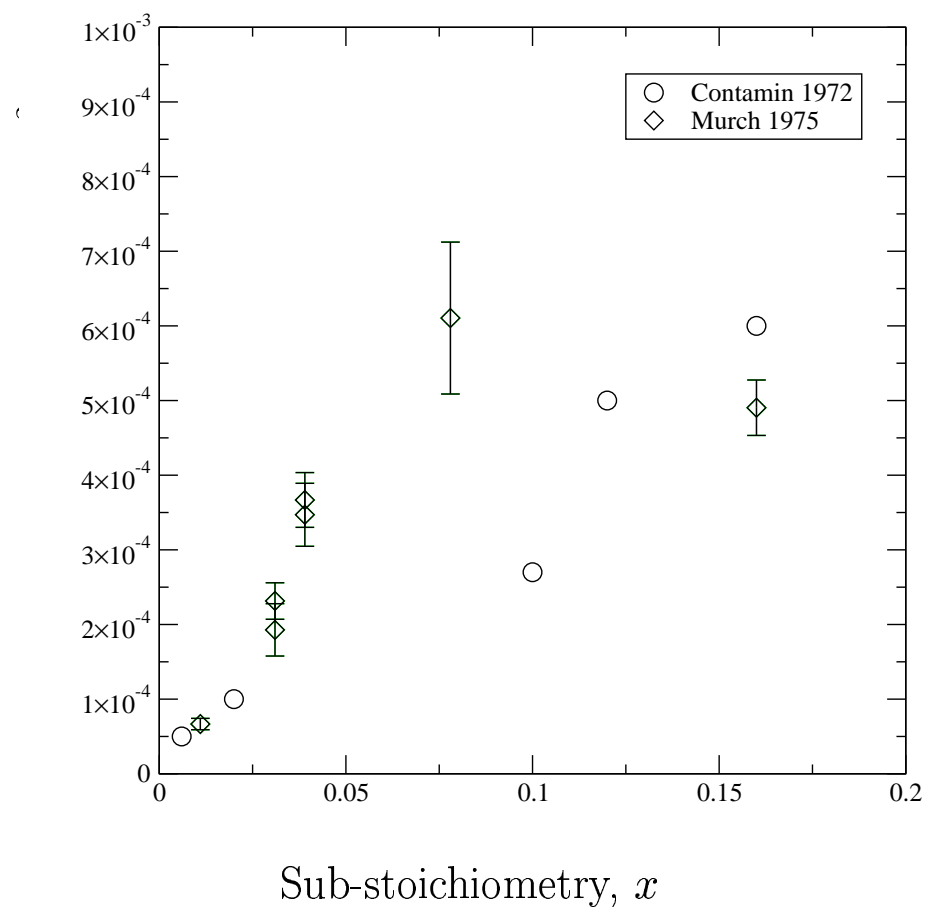


Figure 5.2: D_0 as a function of sub-stoichiometry x taken from Contamin *et al.* [62] and Murch *et al.* [63].

Figure 5.2 is qualitatively very good compared with most migration data, the quality is not sufficient to make any conclusion regarding the sign of ΔH_S . Regardless of the sign of ΔH_S , the Debye frequency, ν , derived from the data plotted in Figure 5.2 using equation 5.6 is predicted to be approximately 10^{13} Hz; a very reasonable value.

Formation enthalpies of intrinsic defects

Table 5.5 shows the intrinsic defect creation enthalpies as a function of stoichiometry for both potential model I and II. Although the exact numbers predicted by potentials I and II differ, both potentials essentially predict the same behaviour. Both models predict that the $\{V_U'''' : U_U^\bullet\}$ may be of importance in UO_{2+x} . The significance of the low V_U'''' enthalpy in UO_{2+x} has been examined in the previous section. In the non-stoichiometric cases the defect concentrations are controlled by the extent of the non-stoichiometry x , the relative solution energies and charge neutrality considerations.

UO_{2-x} In hypo-stoichiometric UO_{2-x} the availability of oxygen vacancies facilitates a simple vacancy assisted oxygen migration mechanism. However, the Schottky disorder enthalpy is high (> 10 eV) and uranium vacancies will not be abundant. This will result in a high predicted cation migration enthalpy in the Arrhenius equation. Uranium ions with an additional electron charge (U^{3+}) are present and may perturb the defect equilibria or the migration processes.

UO_2 In the stoichiometric material the Frenkel equilibrium is responsible for the provision of oxygen vacancies and interstitials. The Frenkel formation energy is predicted to be 3.2-3.4 eV per defect. The Schottky energy is affected by the change in the UO_2 stoichiometry because the Frenkel reaction is the lowest energy intrinsic

Defect	Potential I			Potential II		
	Stoichiometry			Stoichiometry		
	$x < 0$	$x = 0$	$x > 0$	$x < 0$	$x = 0$	$x > 0$
$\text{V}_{\text{O}}^{\bullet\bullet}$	0.00	3.39	6.77	0.00	3.18	6.35
O_{i}''	6.77	3.39	0.00	6.35	3.18	0.00
V_{U}''''	13.23	6.46	-0.31	10.62	4.27	-2.08
$\{\text{V}_{\text{U}}'''' : \text{O}_{\text{i}}''\}$	21.62	11.47	1.30	17.42	7.88	-1.70
$\{\text{V}_{\text{U}}'''' : \text{O}_{\text{i}}''\}_2$	21.30	11.14	0.98	17.85	8.27	-1.30
$\{\text{V}_{\text{U}}'''' : \text{V}_{\text{O}}^{\bullet\bullet}\}$	10.17	6.75	3.37	8.27	5.09	1.92
$\{\text{V}_{\text{U}}'''' : \text{U}_{\text{U}}^{\bullet}\}$	-	7.29	-1.26	-	-	-2.86

Table 5.5: The effective equilibrium formation enthalpies of intrinsic defects in $\text{UO}_{2\pm x}$. The combined defect clusters such as the first and second neighbour $\{\text{V}_{\text{U}}'''' : \text{O}_{\text{i}}''\}$ and $\{\text{V}_{\text{U}}'''' : \text{O}_{\text{i}}''\}_2$ are reported here because migration mechanisms involving those defects are studied later on in this thesis. The $\{\text{V}_{\text{U}}'''' : \text{U}_{\text{U}}^{\bullet}\}$ calculations suggest that in UO_{2+x} the dominant defect is a uranium vacancy with a electronic defect next to it.

defect process.

Although not reported in Table 5.5, the electronic equivalent of the Frenkel defect, the polaron, has a predicted equilibrium formation enthalpy of 3.5 eV.

UO_{2+x} For hyper-stoichiometric UO_{2+x} oxygen interstitials and uranium vacancies are readily available. The calculations predict that Schottky disorder becomes dominant, but the enthalpy advantage is small and inaccuracies in this predicted enthalpy have a large effect on the final defect concentrations. For the migration calculations we will assume that oxygen interstitials and uranium vacancies are available.

5.1.6 Electronic defects

Electronic defects in UO_2 may have a significant influence on migration. It has long been argued that in general ions with a lower absolute charge state have a lower migration enthalpy. In stoichiometric UO_2 both U^{3+} and U^{5+} are available (see Table 5.5). In hypo-stoichiometric UO_{2-x} U'_{U} defects compensate for the lack of oxygen ions. In UO_{2+x} $\text{U}^{\bullet}_{\text{U}}$ defects compensate for the additional oxygen interstitials. In non-stoichiometric oxides the abundance of electronic defects is proportional to the non-stoichiometry (x).

5.1.7 Intrinsic defect mobility

Intrinsic defect mobility is an important parameter in fission product behaviour. The mechanisms by which many large fission products migrate rely on the fast motion of oxygen vacancies or are controlled by slow uranium vacancy migration (see later in this chapter).

The migration of intrinsic defects has been studied with both potential sets. The quasi harmonic approximation has been used to predict the migration enthalpies.

Oxygen vacancies

The vacancy assisted migration of oxygen ions through UO_{2-x} is simple to model, as the migration takes place along one of the lattice vectors (See Figure 5.3).

Simulation of this migration mechanism results in is the migration enthalpy profile in Figure 5.4, with an associated migration enthalpy of 0.7 eV. To test whether the maximum in Figure 5.4 is a saddle point, additional simulations have been performed where the ion is placed at a number of positions on a plane perpendicular to the migration direction. The result of such a simulation is plotted in Figure 5.5 where the axes represent the position and colour is used to show the defect configuration enthalpy. Clearly the migrating ion prefers to move through the center of the plane.

In stoichiometric UO_2 the equilibrium creation enthalpy of an oxygen vacancy needs to be added to the oxygen migration enthalpy and thus an Arrhenius energy of 4.1 eV for oxygen vacancy migration is predicted.

Oxygen interstitials

Since the population of interstitials is really defined by the non-stoichiometry of the oxide, the pre-exponential factor in the diffusion equation is proportional to x or \sqrt{x} (See Section 5.1.5). The activated process is then dependent on the activation enthalpy for interstitial migration from one site to an adjacent site. In the UO_2 structure interstitials move in a $[110]$ direction. As this path leads the migrating ion very close to two lattice anions, a deflection from a straight path is expected.

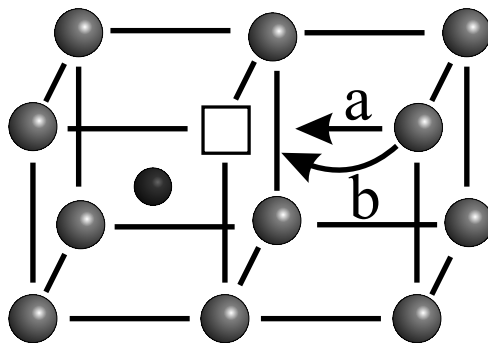


Figure 5.3: Schematic diagram of oxygen migration in UO_2 via an oxygen vacancy mechanism. The migration path could be straight (a) or deflected towards the interstitial site (b). To find out which path is used an additional migration simulation in two dimensions is necessary.

With regard to a $[110]$ migration direction, the ion is expected to deflect but remain in the (001) plane. The nearby ions are deflected roughly in the (001) direction. Simulation of the total energy of the interstitial ion at different sites in the (001) plane are presented in Figure 5.6. The migration enthalpy can be determined from the contour lines and is approximately 3.0 eV.

Uranium vacancies

The migration of uranium between two lattice sites via a cation vacancy is different to the oxygen migration mechanism described in section 5.1.7. Whereas the oxygen migration path goes between two uranium ions which are approximately 1.2 Å apart (based on ionic radii taken from Shannon [105]), uranium ions need to pass between two oxygen ions which are essentially in contact. This means that the migrating uranium ion will be either deflected from a straight line path, force the oxygen ions outwards or both. Both types of lattice displacements are energetically costly.

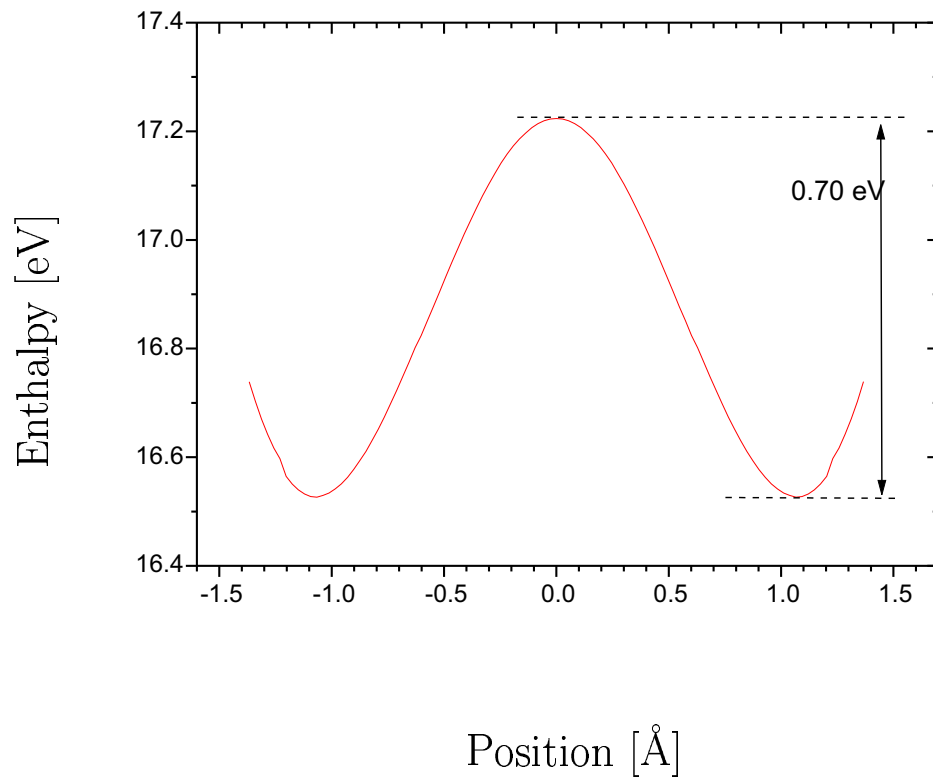


Figure 5.4: The migration enthalpy of an oxygen ion moving between two lattice sites. The boundaries of the graph are on two lattice sites. The two minima of the graph do not coincide with these sites, because the oxygen ion will tend to move towards the nearby vacancy (lattice relaxation).

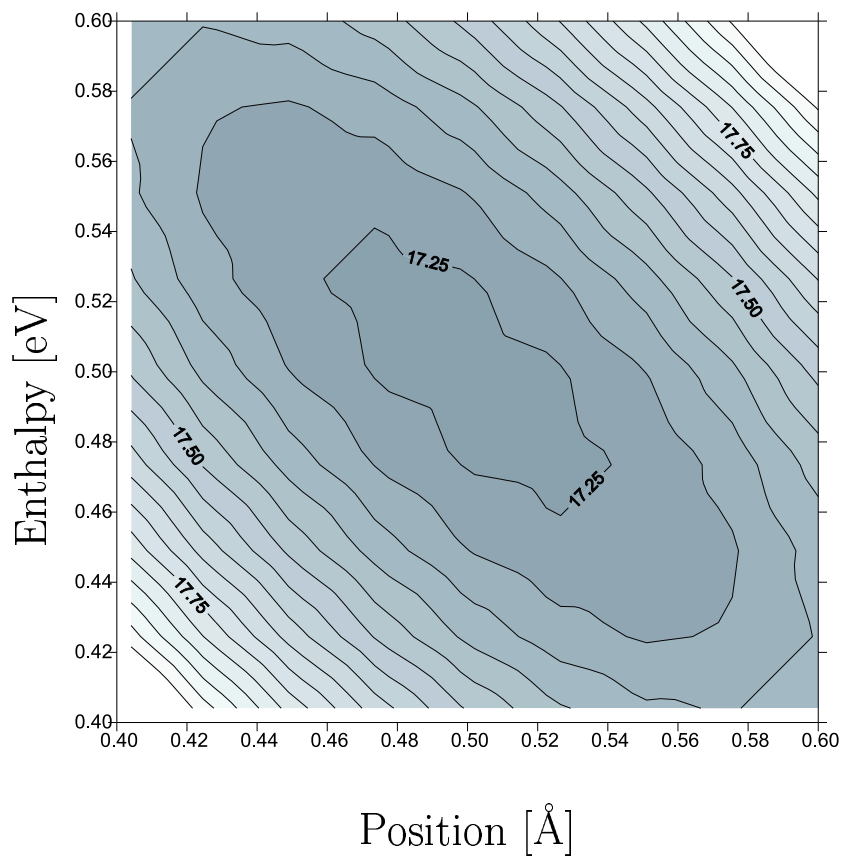


Figure 5.5: The defect energy of an oxygen ion positioned on a plane perpendicular to the migration direction between two vacant oxygen sites. This clearly shows that the ion prefers to go through the middle of the plane. The hypothesis that oxygen ions follow a straight migration path is therefore consistent with the calculations.

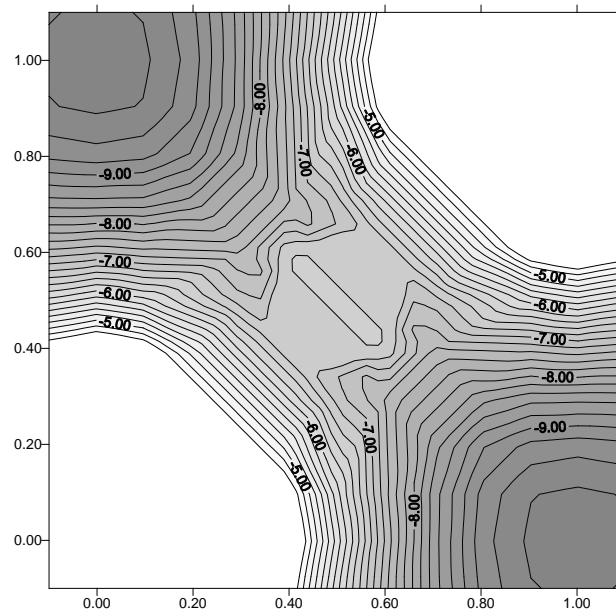


Figure 5.6: The migration of an oxygen interstitial in the UO_2 lattice. The activation energy for this process is approximately 3.0 eV.

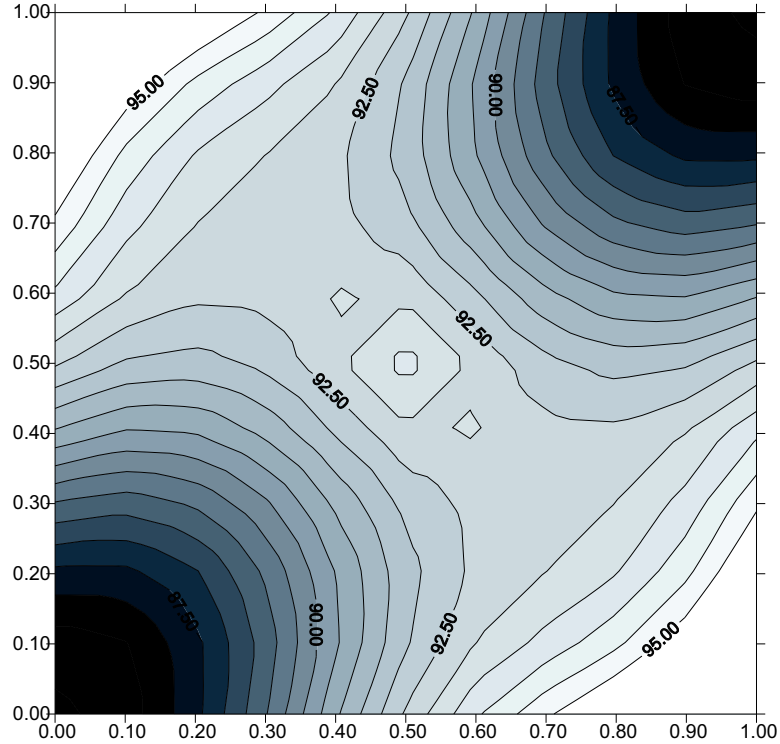


Figure 5.7: This contour map shows the defect enthalpy of a uranium ion as a function of its position on a plane between two lattice sites.

To investigate these two possibilities we have simulated a large number of configurations with the migrating uranium ion moving over a plane which lies between the two equilibrium uranium lattice sites. Our analysis begins by assuming that the uranium ion migrates along this plane. Figure 5.7 shows a plot of the enthalpy as a function of uranium position on the plane. It is clear that uranium is deflected from a straight line migration path as it passes over the saddle point.

To test whether uranium moves out of plane during migration we have plotted the enthalpy on a plane perpendicular to the migration path at the saddle point. It is clear from Figure 5.8 that it does not move out of plane. The migration enthalpy for the mechanism is 6.9 eV. This is a high migration enthalpy compared with the

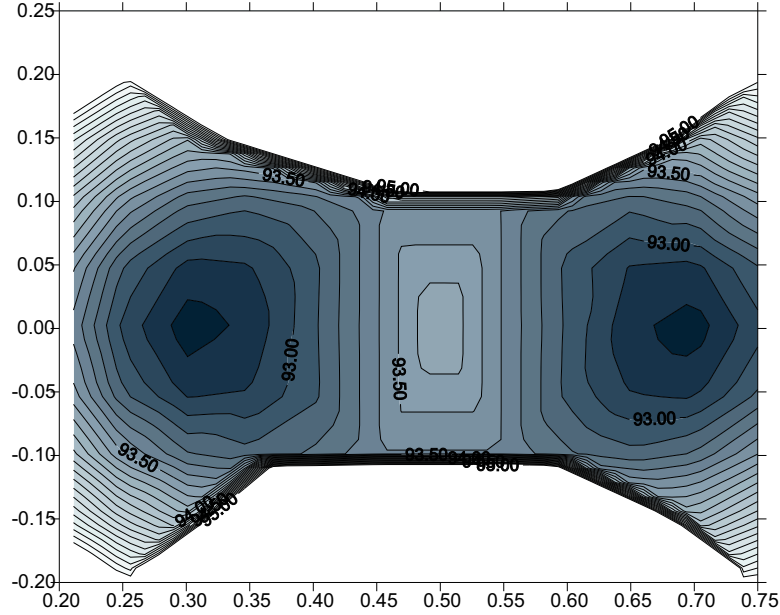


Figure 5.8: In order to find out whether uranium migrates through the plane shown in Figure 5.7, a plane perpendicular to the migration direction has also been simulated. The minimum pathway lies through the dark areas of this plot, which both lie on the simulated migration plane of Figure 5.7.

experimental values [64], especially if we add the equilibrium formation enthalpy of the assisting defect.

Cation migration has only been studied using the original Grimes and Catlow potentials.

UO_{2+x} In UO_{2+x} oxygen interstitials and electron holes on the uranium sites are present and the migration of uranium ions may well be enhanced near those defects. Oxygen interstitials and cation vacancies do not bind because of their mutual repulsion. However, in UO_{2+x} oxygen interstitials are abundant and the formation enthalpy of $\{V_U'''' : O_i''''\}$ clusters is only a little larger than the formation enthalpy

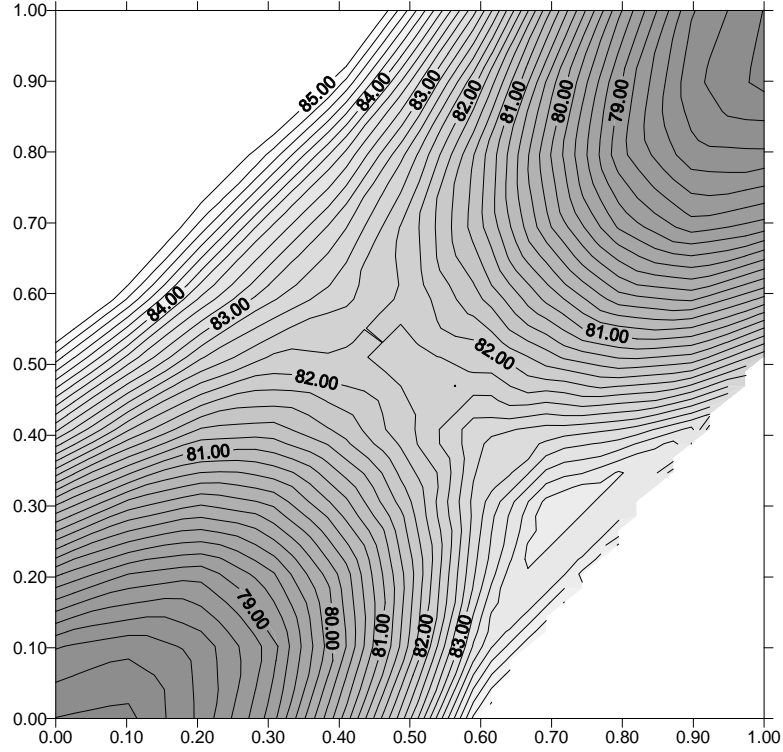


Figure 5.9: The migration of uranium near a first neighbour oxygen interstitial requires 4.54 eV, which is 2.3 eV lower than the migration without the presence of the interstitial. In UO_{2+x} $\{\text{V}_\text{U}^{\prime\prime\prime\prime} : \text{O}_\text{i}^{\prime\prime}\}$ defects will have a significant concentration.

of a uranium vacancy: 1.1 eV for a second neighbour cluster and 1.3 eV for a first neighbour cluster (see Table 5.5). The migration enthalpy of uranium vacancies near such a cluster is lowered as can be seen in Figure 5.9. The first neighbour $\{\text{V}_\text{U}^{\prime\prime\prime\prime} : \text{O}_\text{i}^{\prime\prime}\}^{\prime\prime\prime\prime}$ assisted mechanism yields an Arrhenius migration enthalpy of 5.8 eV for UO_{2+x} which is 1.1 eV lower than the bare cation migration mechanism.

UO_2 Considering the stoichiometric case, the simple $\text{U}_\text{V}^{\prime\prime\prime\prime}$ defect (18 eV), the $\{\text{V}_\text{U}^{\prime\prime\prime\prime} : \text{O}_\text{i}^{\prime\prime}\}^{\prime\prime\prime\prime}$ cluster (15.9 eV) and the $\{\text{V}_\text{U}^{\prime\prime\prime\prime} : \text{V}_\text{O}^{\bullet\bullet}\}^{\prime\prime}$ cluster (13 eV) mechanisms all yield effective Arrhenius energies of > 10 eV. Thus it seems sensible to consider electronic

defects.

In the stoichiometric material the most abundant intrinsic defect that can accommodate uranium migration seems to be the $\{\text{V}_{\text{U}}'''' : \text{U}_{\text{U}}^{\bullet}\}''''$ cluster. The effective Arrhenius migration enthalpy for this process is predicted to be 7.3 eV. This is calculated by adding the formation enthalpy of the cluster in the stoichiometric material and the migration enthalpy in the cluster.

UO_{2-x} Reliable predictions of the uranium self-diffusion activation enthalpies in UO_{2-x} are currently difficult to make, because potentials for 3+ uranium ions have not been derived. 3+ Ions are almost certainly important in the self-diffusion behaviour in UO_{2-x} , especially since the prediction based on what can be simulated now is as high as 16.5 eV. Figure 5.10 shows that the energy of the migration process is only reduced by 0.6 eV when considering an oxygen vacancy bound to the migrating uranium vacancy.

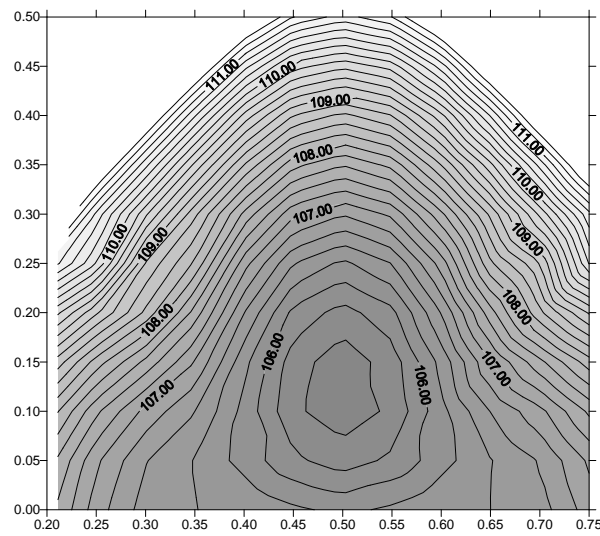


Figure 5.10: By removing a nearby oxygen ion, the migration enthalpy of uranium is reduced by 0.6 eV to 6.3 eV.

5.2 Fission products in UO_2

In this section the behaviour of fission products caesium, iodine [106] and ruthenium [107] is studied in $\text{UO}_{2\pm x}$. The solution process is considered for each possible charge state of the fission product in the three possible stoichiometry states of UO_2 fuel. If the fission product is known only to exhibit a specific charge state, only that charge state is considered in the simulation. However, the predicted charge state of certain fission products will be modified with stoichiometry changes. In such cases (e.g. molybdenum) variation of the fission product charge state is predicted to be energetically favourable over charge state variations of the uranium cation when the stoichiometry changes due to oxidation or reduction [108]. In UO_2 fuel with a high burn-up this can have the effect of increasing the stoichiometry range of the UO_2 , as the formation of e.g. U_4O_9 and U_3O_{8-z} may well depend on the population of U^{5+} ions in the lattice.

In this section the formation enthalpies of complex solution sites are also considered since such sites may play a role in a vacancy assisted diffusion mechanism.

Finally the possible migration paths of the fission products are studied by mapping a route through the lattice and calculating the total energy of the defect with the ion located at consecutive points along the migration route. This type of simulation can be performed in two ways. Either the path is a line through the crystal or it is a curve within a known crystal plane. In the first case it is sufficient to calculate the defect energy for consecutive points along the imaginary line. In the second case the total energy is calculated with the ion located at consecutive points on a grid mapped over a suitable crystallographic plane.

This type of calculation can be extended to perform pathway exploration in materials with complex symmetry by performing simulations on a number of parallel

planes. This results in a 3D pathway and activation energy through this path.

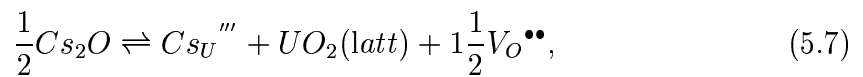
Results of the first type of simulation are plotted on a simple position-energy graph. Results of the second kind are plotted on a contour map, where the total energy is represented by colour and can be read with the help of iso-energy lines [98].

5.2.1 Caesium

Solution

For the first case, caesium solution in $UO_{2\pm x}$, all the steps involved in determining the solution enthalpy as well as the raw calculation data are presented below. (For other fission product ions some of these steps and the raw data will be omitted, mainly because the volume of data is very large and does not contribute to the understanding of the matter.)

If we consider the equilibrium defect reactions between different solution sites and caesium trapped in a di-caesium-oxide precipitate, we can predict which caesium trap will be abundant in the UO_2 lattice, e.g. for a solution mechanism where caesium occupies a uranium vacancy site in UO_{2-x} :



which corresponds with a solution enthalpy of:

$$\Delta H = E_{Cs_U} + E_{L,UO_2} + \frac{1}{2}E_{V_O} - \frac{1}{2}E_{L,Cs_2O} = 9.551[eV], \quad (5.8)$$

where E_{L,UO_2} and E_{L,CsO_2} are the lattice energies of UO_2 and CsO_2 respectively.

To evaluate all reasonable solution mechanisms, it is necessary to define equations like 5.7 for each imaginable trap site and its enthalpy counterpart like equation 5.8.

To account for the fuel stoichiometry Frenkel defects are added or removed from either side of equation 5.7.

In the example above, oxygen vacancies are formed on the right hand side of the equation because the alternative way to fullfill the balance of the equation is to have interstitial oxygen ions on the left. In hypo-stoichiometric UO_2 interstitials are not available.

The defect components of equation 5.8 were simulated with the CASCADE atomic simulation code. The results of the simulation runs are presented in Table 5.6. The numbers in this table refer to single ions taken from infinity and placed in a lattice position or *vice versa*.

Applying solution equations to energies presented in Table 5.6 results in the solution enthalpies for Cs_2O in $\text{UO}_{2\pm x}$, which are shown in Table 5.7. Important solution sites are underlined in this table.

The solution enthalpy predictions in Table 5.7 deviate slightly from those published by Grimes and Catlow [100], as the results presented here are based on simulations which incorporated more ions and slightly different simulation parameters.

Caesium is predicted to be insoluble in UO_{2-x} and UO_2 , but becomes soluble in UO_{2+x} as the uranium vacancy sites necessary to accommodate caesium are more easily formed.

Calculated Cs filled defect energies in UO_2			
Formation energies			
Defect	Defect	Trap	Incorporation energies [eV]
Interstitial	9.957		9.957
Single Cation vacancy			
Cs_U	79.731	85.776	-6.045
Cs_{UO}	93.493	99.134	-5.641
Cs_{UO_2}	108.279	112.923	-4.644
	108.153	113.101	-4.948
	108.480	113.924	-5.444
Double Cation Vacancies			
Cs_{U_2}	168.849	176.619	-7.770
Cs_{U_2O}	178.597	185.732	-7.135
$Cs_{U_2O_2}$	189.274	195.846	-6.572
$Cs_{U_2O_4}$	219.608	224.592	-4.984
	218.632	224.592	-5.960

Table 5.6: Calculated incorporation energies of Cs filled defects in UO_2 . The incorporation energy is defined as the difference between the Cs filled defect and the unfilled trap formation energy. The notation (e.g. $Cs_{U_2O_4}$) refers to caesium trapped in a $\{2 V_U:2 V_O\}$ trap.

Cs solution in equilibrium with Cs_2O precipitate.			
Defect	Solution enthalpy [eV]		
	$x < 0$	$x = 0$	$x > 0$
Cs_U	9.55	<u>4.47</u>	<u>-0.61</u>
Cs_{UO}	6.80	5.11	3.42
Cs_{UO_2}	<u>5.08</u>	6.77	8.47
Cs_{U_2}	26.12	14.27	<u>2.42</u>
Cs_{U_2O}	19.37	10.90	<u>2.43</u>
$\text{Cs}_{U_2O_2}$	13.47	<u>8.49</u>	3.41
$\text{Cs}_{U_2O_4} - \alpha$	<u>9.87</u>	11.57	13.26
$\text{Cs}_{U_2O_4} - \beta$	10.85	12.54	14.24

Table 5.7: Cs solution equilibrium energy per caesium atom. All defects are symmetric, except for the $\text{Cs}_{U_2O_4}$ cluster, which can exist in two states, α and β , depending on which position the impurity occupies inside the cluster.

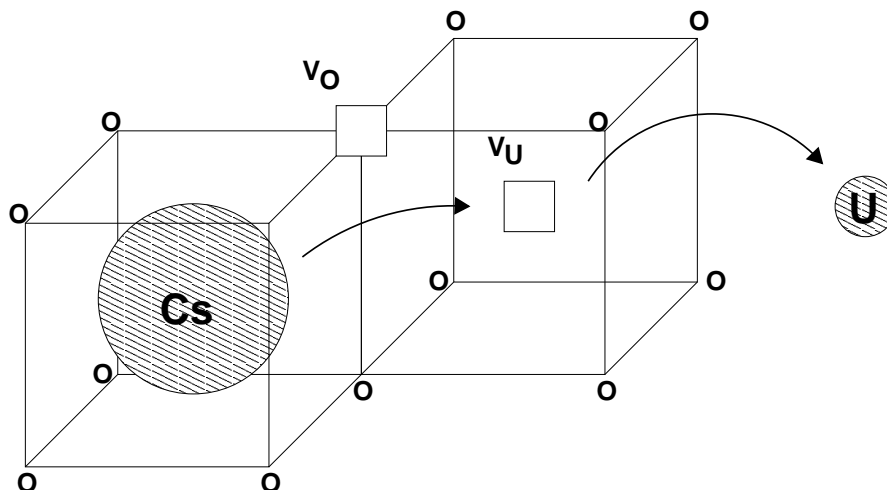


Figure 5.11: The cation vacancy assisted migration mechanism by which Cs migrates in UO_{2+x} . This mechanism is also responsible for iodine migration in UO_{2+x} .

Migration

Caesium migration in UO_{2-x} can occur via the association of one additional uranium vacancy and possibly one or two oxygen vacancies to the Cs_{UO_2} equilibrium trap site. An internal migration step and the loss of the uranium vacancy complete the migration process. The three steps of this mechanism are shown schematically in Figure 5.11.

The formation of a large $\text{Cs}_{\text{U}_2\text{O}_4}$ trap requires between 4.8 and 5.8 eV, depending on the coordination of the oxygen vacancies. The internal migration step is asymmetric and has an activation energy of 1.1 eV (see Figure 5.12) and the most likely migration process is therefore predicted to have an overall migration activation enthalpy of 5.9 eV. However, the activation enthalpy for the self-diffusion of uranium vacancies in UO_{2-x} is 5-7.8 eV (see Table 4.2 on page 72 or Ref. [64]), depending on the stoichiometry, implying that this is the rate determining step.

In stoichiometric UO_2 a similar process is responsible for caesium migration

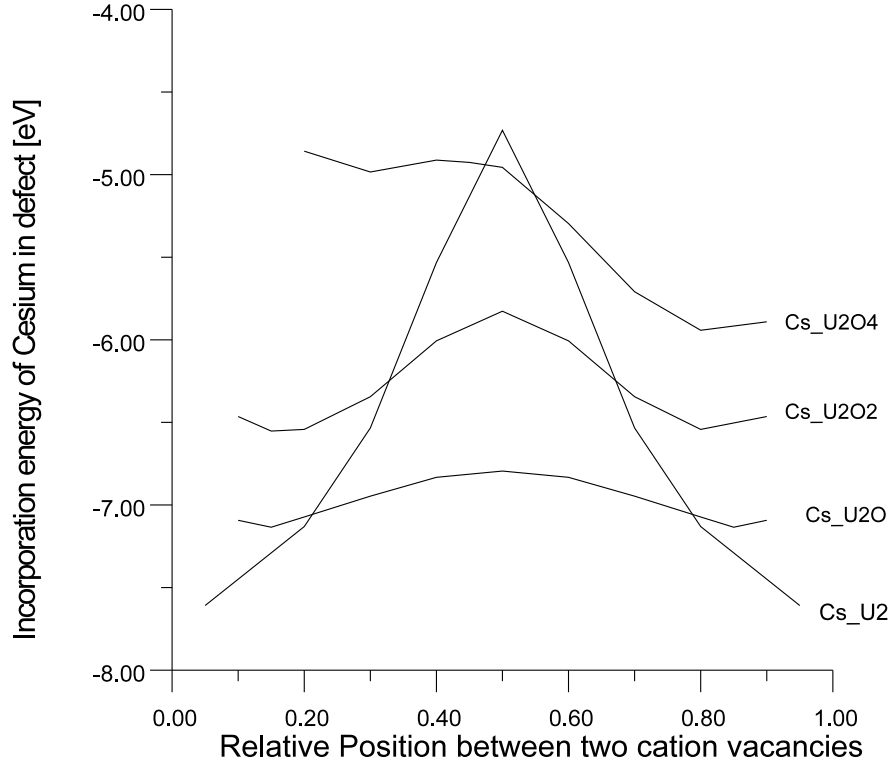


Figure 5.12: Diffusion of caesium inside diffusion clusters. Note that ion diffusion in $\text{V}_{\text{U}_2\text{O}_4}$ is asymmetric.

although in this case the caesium ion equilibrium trap site is a single uranium vacancy. The association of a uranium vacancy and two oxygen vacancies results in a $\text{Cs}_{\text{U}_2\text{O}_2}$ cluster which has a relative formation enthalpy of 4.0 eV and an internal caesium migration enthalpy of 0.7 eV. The predicted total energy is therefore 4.7 eV, which is lower than the migration enthalpy of uranium vacancies (5.6 eV) on which this mechanism should then depend.

In UO_{2+x} migration depends more markedly on the internal migration step. Even though the formation enthalpy of a caesium ion trapped in a uranium di-vacancy is lower than that of a tri-vacancy (which has an added oxygen vacancy), the latter is responsible for caesium diffusion as the internal migration enthalpy is greatly

Caesium	UO_{2-x}	UO_2	UO_{2+x}
ΔH_S	4.96 eV	4.47 eV	-0.61 eV
Trap	$Cs_{UO_2}^\bullet$	Cs_U'''	Cs_U'''
Migration mechanism	Via $Cs_{U_2O_4}^\bullet$	Via $Cs_{U_2O_2}'''$	Via Cs_{U_2O}''''
Process ΔH_M	5.9 eV	4.7 eV	3.4 eV
Rate determining step	Depends on x .	U self-diffusion	Migration process
Predicted ΔH_M	5.9-7.8 eV	5.6 eV	3.4 eV

Table 5.8: Predicted solution enthalpies and migration activation enthalpies of caesium in UO_2 as a function of stoichiometry.

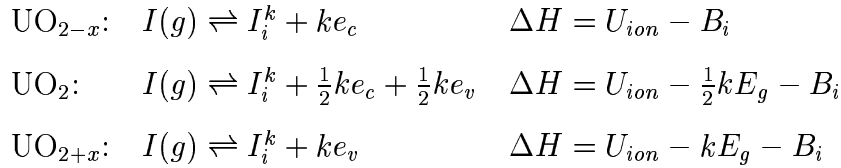
reduced by the additional oxygen vacancy. The total migration process requires 3.4 eV (which is higher than the enthalpy for uranium self-diffusion in UO_{2+x} : 2.6 eV).

Table 5.8. summarises the simulated results for Cs_2O solution in UO_{2-x} , UO_2 and UO_{2+x} . For each ion and range of stoichiometry, the solution enthalpy, solution site, proposed migration mechanism and migration enthalpy are reported.

5.2.2 Iodine

Solution

The stoichiometry state of the UO_2 fuel has implications for the charge state of iodine. It is therefore important that this is factored into the solution equations properly. If we consider solution of interstitial iodine from a gaseous state for example:



In these equations k is the ionization state of iodine. The electrons either go into the valence band or the conduction band, which is indicated by e_v and e_c . U_{ion} is the ionization potential taken from Table 5.3 and B the binding energy of the defect. In UO_2 and UO_{2+x} the ionization potential is modified by the fact that electrons from ionizing species end up in the lattice [100]. The electron affinity for this process is equal to $\frac{1}{2}E_g$ in UO_2 and E_g in UO_{2+x} respectively, where E_g is the bandgap (2.3 eV) in UO_2 [57].

Simulations were performed on a large number of possible iodine filled traps in UO_2 and the resulting solution enthalpies are shown in Table 5.9.

In UO_{2-x} the preferred charge state and solution site is I^- in either an oxygen mono- or di-vacancy. I^- has an ionic radius of 2.2 Å [105], which is much larger than that of oxygen (1.42 Å) and this explains the preference for solution in a di-vacancy.

In stoichiometric UO_2 two different solution mechanisms are apparent. Iodine is predicted to assume a I^{2+} charge state and occupies a cation vacancy or assume a I^- charge state and occupy a vacancy cluster consisting of a uranium and one or two oxygen vacancies.

In UO_{2+x} iodine is predicted to occupy uranium vacancy trap sites and exhibit an I^{2+} charge state. Clearly this is the only option in hyper-stoichiometric fuel, as oxygen vacancies and clusters containing both O and U vacancies are energetically unfavourable.

Reiterating the conclusions of Grimes and Catlow [100]:

- Iodine is associated with oxygen vacancies in UO_{2-x} , with uranium and oxygen vacancy complexes in UO_2 and with uranium vacancies in UO_{2+x} .
- The solution enthalpies are clearly reduced when UO_2 is oxidised from the stoichiometric composition.

Solution energies of Iodine in UO_2 (eV)												
	UO_{2-x}				UO_2				UO_{2+x}			
	I^-	I	I^+	I^{2+}	I^-	I	I^+	I^{2+}	I^-	I	I^+	I^{+2}
Interstitial	15.79	17.63	23.42	25.86	15.79	16.48	21.12	22.41	15.79	15.33	18.82	18.96
I_O	<u>8.95</u>	14.23	22.28	27.43	12.34	16.46	23.37	27.37	15.73	18.70	24.45	27.31
I_U	21.99	20.81	20.76	20.62	15.31	12.98	11.79	<u>10.40</u>	8.85	5.06	2.71	<u>0.17</u>
I_{O_2}	<u>7.99</u>	14.30			15.72	19.20			22.49	25.54		
I_{UO}	14.04	17.63			<u>10.66</u>	13.09			7.27	8.55		
I_{UO_2}	10.69	13.18			<u>10.69</u>	12.03			10.69	10.88		
I_{UO_2}	12.65	13.37			12.65	12.22			12.65	11.07		
I_{U_2}			37.24	35.73			21.40	18.73			5.55	1.73

Table 5.9: Solution enthalpies of Iodine in UO_2 .

Note: The blank values are a result of problems associated with the core-shell model. Defect calculations did not properly minimize due to excessive core-shell displacements.

- For iodine, predicted solution enthalpies are evaluated relative to free iodine gas. If compounds containing iodine then form outside the fuel matrix, it is clear that the solution energy will only become less favourable. In the cases of solution in UO_{2-x} and UO_2 such an effect is of no practical significance since the solution enthalpies are already so high (i.e. zero solution). However, in UO_{2+x} , where the solution enthalpy is rather small a modest increase could reduce the solubility of iodine significantly.

An isolated atom in a host lattice is a unique chemical environment where the notional charge states adopted by the atom are governed by energy minimisation within the lattice as a whole. To this end, the possibility of the ‘unusual’ I^{2+} charge state has been considered alongside the more common $\text{I}^-/\text{I}^0/\text{I}^+$. Interestingly, the simulations predict that iodine prefers the I^{2+} charge state in UO_{2+x} . However, due to the residual uncertainty as to whether oxidation beyond I^+ is achieved in practice, the results for both I^+ and I^{2+} charge states are discussed.

Migration

Iodine migration is different from caesium migration as the ion can exhibit a negative formal charge state in which it traps more easily at oxygen vacancies. In UO_{2-x} it is trapped in an oxygen di-vacancy in which it can be in two positions which are separated by a migration barrier of only 0.3 eV. The loss of a vacancy to form an $\text{I}_\text{O}^\bullet$ is a process which requires 1 eV. As the internal migration step occurs at equilibrium, this is not added to the total process energy and the migration enthalpy is therefore predicted to be 1 eV (i.e. higher than the energy for oxygen self-diffusion).

The reduced availability of oxygen vacancies in stoichiometric UO_2 forces the I ion (still with a charge state of -1) to occupy a UO di-vacancy, I_{UO} . The dissociation

Iodine	UO_{2-x}	UO_2	UO_{2+x}
ΔH_S	7.99 eV	10.66 eV	0.17 / 2.71 eV
Charge state	I^-	I^-	$\text{I}^{2+} / \text{I}^+$
Trap	$\{I_O^\bullet : V_O^{\bullet\bullet}\}^{\bullet\bullet\bullet}$	$\{I_O^\bullet : V_U^{\bullet\bullet\bullet}\}^{\bullet\bullet\bullet}$	$I_U^{\bullet\bullet} / I_U^{\bullet\bullet\bullet}$
Migration mechanism	Via I_O^\bullet	Via I_O and I_{UO_2}	Via $I_{\text{U}_2\text{O}}$
Process ΔH_M	1.0 eV	1.7 eV	5.1 eV / 6.3 eV
Rate determining step	I_O^\bullet formation	U self-diffusion	Internal migration
Predicted ΔH_M	1.0 eV	5.6 eV	5.1 eV / 6.3 eV

Table 5.10: Predicted solution enthalpies and migration activation enthalpies of iodine in UO_2 as a function of stoichiometry.

and association of uranium and oxygen vacancies is responsible for the migration although, unlike Cs, I does not need a V_{U_2} cluster to migrate as it can occupy a single oxygen vacancy. Dissociation of the uranium vacancy from the oxygen vacancy trap requires 1.7 eV. The uranium self-diffusion (5.6 eV) therefore controls the process. Despite the much larger process energy due to the necessity for uranium self-diffusion the alternative, where iodine migrates via oxygen vacancies, has an even higher energy.

Assuming that iodine ionizes to I^{2+} in UO_{2+x} , the formation of a di-uranium vacancy from the I_U trap requires 1.6 eV. The internal migration step expends a further 3.5 eV and the predicted migration enthalpy would be 5.1 eV.

If we assume that iodine only ionises to I^+ in UO_{2+x} then the mechanism is the same, but the formation of the di-vacancy requires 2.8 eV and the total process energy is 6.3 eV.

An overview of these results is shown in Table 5.10.

In the Arrhenius diffusion equation,

$$D(T) = d^2 \nu \exp\left(\frac{-E_M}{k_B T}\right), \quad (5.9)$$

the value we attempt to predict via these atomistic simulations is E_M . The assumption here is that diffusion is via the motion of ionic species which means that appropriate estimates for the length of the jump step, d , and the attempt frequency, ν , can be made. The jumpstep in UO_2 is approx. 2.5-4 Å and the attempt frequency is usually given as 10^{11} to 10^{14} . $D_0 \approx d^2 \nu$ can therefore be estimated to be 10^{-5} to 10^{-1} [cm^2/s] for UO_2 . If we compare the values for D_0 in Table 4.3 then it is clear that the Arrhenius equations for Cs correspond well with the suggested interval for D_0 . However, the D_0 values fitted to iodine experiments show 15 orders of magnitude variation. The results of Prussin *et al.* show a rather high D_0 whereas those of Friskney suggest a rather low D_0 , both slightly outside of the range we would expect from a theoretical point of view.

Figure 5.13. shows the Arrhenius equation for 5.6 eV plotted over the available data. The assumed D_0 value is $10 \text{ cm}^2/\text{s}$ which is higher than expected from a theoretical point of view.

5.2.3 Concluding comments

Caesium and iodine are practically insoluble in UO_2 and UO_{2-x} . Furthermore, although both ions show an important reduction of the solution enthalpy in UO_{2+x} , only Cs seems to show any appreciable solubility upon oxidation of the UO_2 lattice.

The experimental activation enthalpy for Cs migration in UO_2 (4.3 eV) is lower than the uranium activation enthalpy for self-diffusion (5.6 eV), which is predicted to be the controlling step in the migration mechanism. If the process were not to depend on the uranium migration, which is possible if, for example, uranium diffusivity

were greatly enhanced by radiation damage, then the predicted migration enthalpy would be 4.7 eV. The experimental data summarised in Figure 4.4 is certainly consistent with this hypothesis and both sets of experimental data were derived from highly irradiated materials (i. e. materials which are likely to have uranium vacancy concentrations elevated above those at equilibrium).

The comparison of the predicted iodine activation enthalpy with the experimental data in Figure 5.13 shows very good agreement with the trace irradiated post-irradiation results of Prussin *et al.* [7]. Under irradiation conditions with moderate burn-up the migration process seems to proceed via a different mechanism, as the Friskney and Turnbull [53] results show.

One implication of these differences is that irradiation damage can simultaneously affect the diffusion mechanism, by creating non-equilibrium concentrations of defects that provide migration mechanisms with lower activation energies. The current model can be used to consider such processes as the simulation model can predict activation energies associated with trap sites and defect association. Clearly such further investigation would be usefull since it is the in-pile results of Friskney and Turnbull which would appear relevant for reactor safety studies.

5.2.4 Ruthenium

Ruthenium has been observed experimentally in UO_2 as a constituent of the five-metal particle [16,18] and at the surface in the form of various ruthenium oxides [83]. Since the precipitation of the five-metal particle and the release process of ruthenium both involve atomic diffusion, ruthenium must also exist in solution in the UO_2 matrix.

In the event of a containment failure which results in the exposure of hot fuel

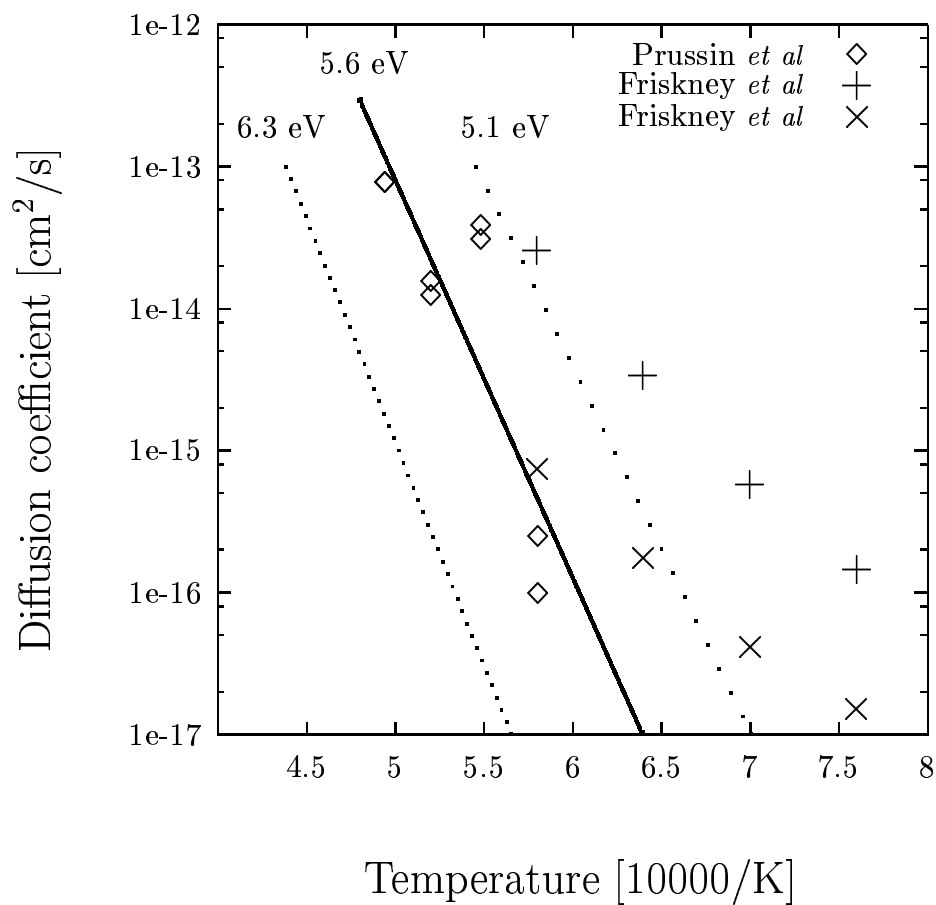


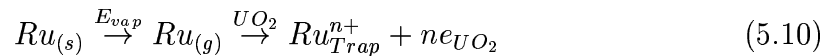
Figure 5.13: Comparison of the suggested migration activation enthalpies for iodine with literature data [7, 53]. The three lines correspond with the possible predictions for the Arrhenius enthalpy for UO_2 and UO_{2+x} . This figure shows that a value of 5.6 eV is a good prediction for the high temperature ex-pile diffusion in UO_2 .

to an oxidising atmosphere, progressive oxidation of $UO_2 \rightarrow UO_{2+x} \rightarrow U_4O_9 \rightarrow U_3O_{8-z}$ can occur, with the stable phase being determined by the atmosphere and temperature. Experimental work [83] shows that ruthenium appears at the surface and oxidizes to the volatiles RuO_3 and RuO_4 , both of which may leave the surface of U_3O_8 .

Ruthenium metal solution in UO_2

Here we report solution energies of ruthenium in a variety of charge states in UO_{2-x} , UO_2 and UO_{2+x} . Eight possible trap sites are considered including simple substitution at a uranium site, substitution at complex vacancy clusters and interstitial solution. This data is then used to determine possible migration mechanisms and finally the predicted activation energy.

In the first instance solution of ruthenium will be determined with reference to the metal. The first term in calculating the internal energy of solution is the enthalpy of vapourization of ruthenium metal; $E_{vap} = 6.72$ eV per metal atom [109]. Equation 5.10 shows the process of metal solution of Ru in UO_2 .



The ruthenium ion will assume a charge state that minimises the total energy. Thus the ionization energies of isolated ruthenium atoms (Table 5.3) must also be included in the energy balance. The ionization energy is adjusted for the fact that the electrons do not go to infinity, but are absorbed by the lattice upon ion solution. This correction, which is the electron affinity E_{aff} of UO_2 , depends on the stoichiometry. Following previous calculations (see Section 5.2.2 or Ref. [100]), in UO_{2-x} this is zero, in UO_{2+x} $E_{aff} = 2.3$ eV (the band gap energy) and in UO_2 , E_{aff}

= 1.15 eV (half the band gap). The trapping of ruthenium at a trap site follows the usual rules of charge neutrality and conservation of mass and the creation of intrinsic defects to satisfy those laws.

The enthalpies for ruthenium solution with respect to the metal are presented in Table 5.11. In previous studies, atoms such as Xe and Cs [100] have shown preference for the neutral tri-vacancy. Here solution is favoured in smaller sites: in UO_{2-x} , Ru^{2+} in a V_{UO} , in UO_2 and UO_{2+x} as Ru^{3+} in a uranium vacancy. The highest predicted ruthenium charge state is 3+. This reflects the value of the fourth ionization energy of ruthenium [103] (47.96 eV) compared to uranium [58] (31.06 eV). The magnitude of the electrostatic Madelung field in UO_2 is simply not sufficient to promote the fourth ionization of ruthenium and in fact even the fifth ionization energy of uranium is predicted to be only 45.77 eV [58].

By considering the sign and magnitude of the solution energies in Table 5.11, it is also clear that solution in UO_{2-x} is not favoured with respect to the metal, in agreement with the observed formation of α -Ru particles. However, solution is strongly favoured in UO_{2+x} . and thus ruthenium should prefer to remain in solution under oxidising conditions. Given the magnitude of the negative solution energy in UO_{2+x} it is possible that metal particles will begin to undergo resolution.

Ruthenium-oxide solution in UO_2

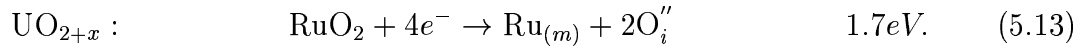
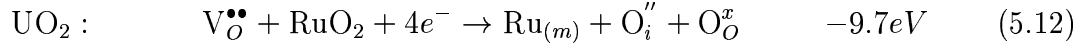
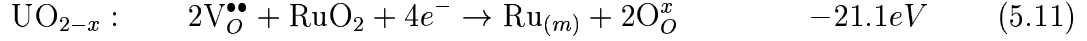
In the previous section ruthenium solution was compared with ruthenium in a metal particle, since these particles are observed in experimental work [16, 18]. The theoretical results support a preference for metal precipitation in UO_2 and UO_{2-x} .

However, in UO_{2+x} the metal was predicted to be soluble, effectively due to the higher oxygen potential. This then begs the question: What is the likelihood of RuO_2

Solution enthalpies of Ruthenium in $UO_{2\pm x}$ (eV)															
	UO_{2-x}					UO_2					UO_{2+x}				
	Ru	Ru^+	Ru^{2+}	Ru^{3+}	Ru^{4+}	Ru	Ru^+	Ru^{2+}	Ru^{3+}	Ru^{4+}	Ru	Ru^+	Ru^{2+}	Ru^{3+}	Ru^{4+}
Int.	24.9	18.9	18.1	20.7	26.8	24.9	17.8	15.8	17.3	22.2	24.9	16.6	13.5	13.8	17.6
Ru_O	22.8	19.7	21.0	24.9	31.0	26.2	21.9	22.1	24.9	29.8	29.6	24.2	23.3	24.9	28.6
Ru_U	24.4	17.3	14.8	15.8	23.1	17.6	9.4	<u>5.7</u>	<u>5.6</u>	11.6	10.8	1.4	-3.4	<u>-4.7</u>	0.2
Ru_{UO}	20.9	15.0	<u>13.4</u>	15.0	21.8	17.5	10.5	7.7	8.1	13.8	14.1	5.9	2.0	1.3	5.8
Ru_{UO_2}	18.8	14.3	13.8	16.1	22.9	18.8	13.2	11.5	12.6	18.3	18.8	12.0	9.2	9.2	13.7
Ru_{U_2}	42.3	34.1	30.4	30.3	36.2	28.7	19.3	14.5	13.2	18.0	15.1	4.6	-1.4	-3.9	-0.2
Ru_{U_2O}	34.6	27.8	25.3	26.0	31.9	24.4	16.5	12.8	12.3	17.1	14.2	5.1	0.3	-1.3	2.3
$Ru_{U_2O_2}$	27.7	22.7	21.5	23.1	29.4	20.9	14.7	12.3	12.9	18.0	14.1	6.8	3.2	2.6	6.6

Table 5.11: Solution enthalpies of ruthenium in $UO_{2\pm x}$, relative to ruthenium metal. The preferred solution sites for each UO_2 stoichiometry are underlined.

precipitation in UO_{2+x} ? The answer to this question can be found by calculating the enthalpies involved in the reduction of RuO_2 to $Ru_{(m)}$ within $UO_{2\pm x}$. A reduction or oxidation within the lattice will always depend on the oxygen potential of the environment which is controlled by the fuel stoichiometry:



All the enthalpies in equation 5.11-5.13 have been calculated with CASCADE and the ionization potentials are taken from Table 5.3 and corrected for the band-gap.

The results for UO_{2-x} and UO_2 imply that any RuO_2 present will have its oxygen removed by the fuel lattice and Ru metal will be formed. In UO_{2+x} the oxide RuO_2 is stable with respect to the metal. However the additional stability resulting from ruthenium being in an oxide is not sufficient to remove ruthenium from solution within the lattice (i. e. 1.7 eV from equation 5.13 is less than 4.7 eV, the solution energy for ruthenium in UO_{2+x} from Table 5.11).

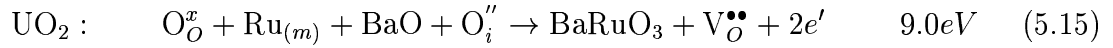
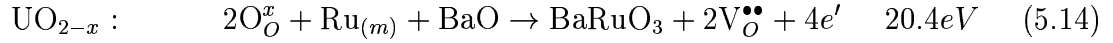
Clearly ruthenium oxide precipitates are not preferred at all in UO_{2-x} and UO_2 and are not likely in UO_{2+x} .

Formation of $BaRuO_3$

Although metal particles may be soluble in UO_{2+x} it is possible, given the elevated oxygen partial pressure, that the available ruthenium is incorporated into a secondary oxide phase different than that of the fuel matrix or RuO_2 . For example, many fission products are incorporated into grey phase particles [16] that are essentially substituted barium zirconate perovskite. Thus a representative second oxide

phase to consider would be BaRuO_3 although formation of RuO_2 and $\text{Ru}_{(m)}$ phases and solution in the host lattice should also be considered since the fission yield of barium is less than that of ruthenium [100].

The reactions responsible for the formation of BaRuO_3 can be constructed relative to the most likely ruthenium and barium state in UO_2 :



BaRuO_3 exhibits a nine layer rhomboherdral structure (9R) related to perovskite [102, 110, 111], rather than a simple cubic perovskite. We correctly predict the rhomboherdral structure to be lower in energy than the cubic polymorph and a negative reaction enthalpy when RuO_2 and BaO form BaRuO_3 ($\Delta E = -0.69\text{eV}$). The predicted unit cell parameters are $a = 5.962$ and $c = 22.196$, where the experimental values are $a = 5.75$ and $c = 21.60$. This equates to a 10% error in the lattice volume. More modern potentials perform better here, but for the sake of consistency Ba and Ru potentials compatible with the original Catlow and Grimes set are used. The energy predictions of these simulations have been substituted into equations 5.14-5.16.

Figure 5.14 and Table 5.12 summarize the solution mechanisms considered above. The figure shows the solution enthalpies re-normalized for the lowest solution site or mechanism. BaRuO_3 has been included in this figure with the understanding that this picture is only valid for the situation in which ruthenium is produced at a higher rate than barium, which is true in normal UO_2 fuel (Figure 1.3). Clearly

Summary of ruthenium accomodation mechanisms			
	UO_{2-x}	UO_2	UO_{2+x}
Mechanism	Solution enthalpy [eV]		
Metallic precipitate	0	0	4.6
Solution in UO_2 lattice	13.4	5.6	0
RuO_2 precipitate	21.1	9.7	2.9
BaRuO_3 precipitate	20.4	9.0	2.2

Table 5.12: Comparison of ruthenium accomodation mechanisms in UO_2 . The reported energies are relative to the lowest energy in the stoichiometry range.

metallic ruthenium is preferred in UO_{2-x} and the stoichiometric material. In UO_{2+x} the preferred accomodation mechanism is substitutional solution in the fuel matrix.

Ruthenium Migration

Several migration mechanisms have been explored to predict the atomic diffusion behaviour of ruthenium. Depending on the lattice stiochiometry there are fundamentally two methods. In UO_{2-x} migration via an oxygen vacancy is the lowest energy process, whereas in UO_2 and UO_{2+x} uranium vacancies are employed to facilitate migration.

UO_{2-x} From Table 5.11 we can establish that there are few viable low energy solution mechanisms in UO_{2-x} . The formation of a filled double uranium vacancy which plays a role in the stoichiometric and hyperstoichiometric material is highly unlikely, so dissociation of the most stable Ru_{UO} trap into Ru_{O} and V_{U} is the most likely first step of ruthenium migration in UO_{2-x} . This is remarkable, since single uranium vacancies are rare in hypo-stoichiometric UO_2 . The random association of

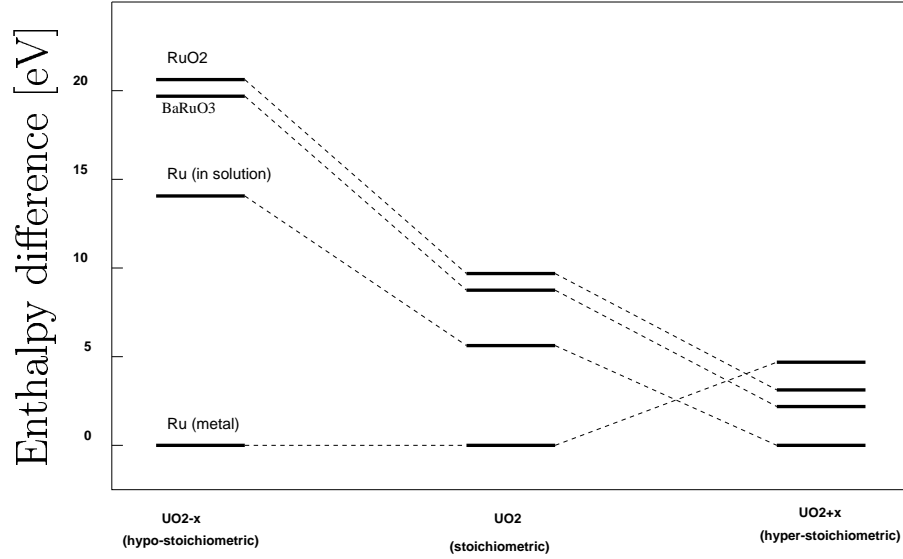


Figure 5.14: Schematic diagram of the accommodation of Ru in UO_2 fuel as a function of stoichiometry.

a uranium vacancy at one of four neighbouring uranium sites finalizes the migration mechanism. This mechanism is only possible due to the large number of oxygen vacancies available.

The energy penalty of this dissociation is 7.6 eV, a value which can be reduced by assuming that the dissociated V_U donates an electron, leaving a Ru_O^+ . The mechanism would result in a 6.3 eV migration enthalpy, assuming that such a charge transfer is possible. The dynamics of such a charge transfer have not been studied here.

UO_2 In stoichiometric UO_2 the formation of a double uranium vacancy, possibly with a number of oxygen vacancies associated with it are candidate migration mechanisms. The overall migration enthalpy is likely to be large, because the difference between the solution enthalpies of the Ru'_U equilibrium site and the most likely Ru''''_{U_2}

site is about 6 eV.

Since a number of trap sites are available and charge transfers seem likely, it is worth studying the migration within Ru_{U_2} , $\text{Ru}_{\text{U}_2\text{O}}$ and $\text{Ru}_{\text{U}_2\text{O}_2}$ for ruthenium charge states +2, +3 and +4.

Without a charge transfer, ruthenium may migrate by means of a $\text{V}_{\text{U}_2\text{O}}$ vacancy in stoichiometric UO_2 . Both the non-equilibrium solution and the migration enthalpies are very high and result in a total migration enthalpy of 13.1 eV. Table 5.13 shows that the internal migration enthalpy for a Ru^{2+} ion is typically 2 eV lower than that of a Ru^{3+} ion. The non-equilibrium solution of a +2 ion in a V_{U_2} like trap is only slightly higher than that of a +3 ion. Thus a charge transfer would lower the energy of the migration process. The optimal process where Ru^{2+} migrates with the aid of a $\text{V}_{\text{U}_2\text{O}_2}$ vacancy cluster has a total migration enthalpy of no less than 11.3 eV.

Note that Table 5.13 also suggests that the commonly held rule that higher charge state implies higher activation energy for migration is not always true.

UO_{2+x} In hyper-stoichiometric the concentration of uranium vacancies is larger than the concentration in stoichiometric UO_2 . The mechanism of migration in UO_{2+x} will therefore be similar to the mechanism in the stoichiometric material.

In contrast with the stoichiometric case presented above, the formation of a double uranium vacancy trap is energetically favourable and thus the overall migration enthalpy is greatly reduced. The advantageous internal migration enthalpy of the Ru^{2+} is offset by a high non-equilibrium solution enthalpy for the +2 ion in a double uranium vacancy. The results in Table 5.11 and Table 5.13 predict that Ru^{3+} inside a double uranium vacancy is responsible for diffusion of ruthenium. The total Arrhenius migration enthalpy for the mechanism is 6.9 eV, most of which is due

Migration of ruthenium ions within V_{U_2} like defects.		
Ruthenium in a V_{U_2} defect		
<u>Ion</u>	<u>Migration enthalpy [eV]</u>	
Ru^{2+}	4.08	
Ru^{3+}	6.12	
Ru^{4+}	5.71	
Ruthenium in a V_{U_2O} defect		
<u>Ion</u>	<u>Migration enthalpy [eV]</u>	
Ru^{2+}	4.24	(4.56)
Ru^{3+}	6.38	(7.17)
Ru^{4+}	6.67	(8.27)
Ruthenium in a $V_{U_2O_2}$ defect		
<u>Ion</u>	<u>Migration enthalpy [eV]</u>	
Ru^{2+}	4.61	
Ru^{3+}	6.20	
Ru^{4+}	9.84	

Table 5.13: Ruthenium migration mechanisms employing uranium and oxygen vacancy clusters. The component enthalpies presented here are the internal migration enthalpies for ruthenium ions within $V_{U_2O_n}$ trap sites. In a Ru_{U_2O} defect the migrating ion strays from the straight line by approximately 0.3-0.4 Å. The values in brackets represent the resulting migration enthalpies if this were not taken into account.

to the internal migration step.

A summary of these results is shown in Table 5.14.

Ruthenium	UO_{2-x}	UO_2	UO_{2+x}
ΔH_S	13.41 eV	5.59 eV	-4.66 eV
Charge state	Ru^{2+}	Ru^{3+}	Ru^{3+}
Trap	$\text{Ru}_{\text{UO}}^{\times}$	Ru'_{U}	Ru'_{U}
Migration mechanism	Via $\text{Ru}_{\text{O}}^{\bullet\bullet\bullet}$	Via $\text{Ru}_{\text{U}_2\text{O}_2}^{2+''}$	Via $\text{Ru}_{\text{U}_2}^{3+''''}$
Process ΔH_M	6.3 eV	11.3 eV	6.9
Rate determining step	$\text{Ru}_{\text{O}}^{+\bullet}$ formation	$\text{Ru}_{\text{U}_2\text{O}_2}^{2+}$ formation + internal migration	Internal migration
Predicted ΔH_M	6.3 eV	11.3 eV	6.9 eV

Table 5.14: Predicted solution enthalpies and migration activation enthalpies of ruthenium in UO_2 . The solution enthalpies are relative to metallic ruthenium.

5.3 U_3O_8

The U_3O_8 structure studied in this section is the hexagonal layered high temperature form ($P\bar{6}2m$). The ionic model proposed by Ball and Dickens [112] is used to represent the lattice. This model assumes a $+5\frac{1}{3}$ charge on the uranium ions and the standard -2 charge on oxygen ions. The physics behind this choice can be explained by assuming that the mobility of an electron hole, that must exist on each third uranium ion, is great enough that it is shared or delocalised over three cations. This view is supported by the $P\bar{6}2m$ hexagonal symmetry of the lattice where all uranium ions are in identical surroundings.

5.3.1 Inter-ionic potentials

The initial potential parameters for U_3O_8 were derived by Ball and Dickens [96] using the electron gas methodology [42]. Since oxygen ions with two distinctly different coordinations can be identified within the U_3O_8 structure, these ion classes were treated separately. This resulted in two slightly different inter-ionic potential sets: one for planar and one for chain oxygen ions. The resulting potentials are tabulated in Table 5.15.

5.3.2 Perfect lattice results for U_3O_8

The “CASCADE” code was used to perform all U_3O_8 simulations. The basic lattice properties are listed in Table 5.16, together with some basic defect energies and existing experimental results. Unfortunately there is little experimental data for the U_3O_8 phase.

The average static and optic dielectric constants (ϵ^0 and ϵ^∞) were calculated

U ₃ O ₈ Buckingham potentials used in this study [112].			
Atoms	A [eV]	ρ [Å]	C [eV Å ⁶]
U ^{+5$\frac{1}{3}$} — U ^{+5$\frac{1}{3}$}	31002.05	0.24421	67.97
O ⁻² — O ⁻²	144.78	0.44141	35.3
OX ⁻² — OX ⁻²	154.30	0.43456	35.3
O ⁻² — OX ⁻²	149.47	0.43842	35.3
U ^{+5$\frac{1}{3}$} — O ⁻²	2963.89	0.34165	48.21
U ^{+5$\frac{1}{3}$} — OX ⁻²	3023.31	0.33889	48.21

Table 5.15: Inter atomic potentials for the U₃O₈ system.

using the effective medium approximation as described by Stroud [113]. The static dielectric constant can be estimated using the empirical relationship of Gladstone and Dale (see R.G. Ball, PhD thesis, 1991, p. 106 [112]). The value predicted by the calculations is in good agreement with this estimated value.

5.3.3 Equilibrium formation enthalpies of intrinsic defects in U₃O₈ and U₃O_{8-z}

Equilibrium intrinsic defect formation enthalpies for U₃O_{8-z} and U₃O₈ are shown in Table 5.17. This shows that the formation enthalpies for cation vacancies in U₃O₈ and U₃O_{8-z} are very high, and a conclusion from this model is that negligible diffusion will take place via uranium cation vacancies. Even in the stoichiometric material the uranium vacancy formation enthalpy is 11.1 eV. Clearly a different mechanism is responsible for uranium diffusion in U₃O₈.

The availability of oxygen vacancies in U₃O_{8-z} makes the formation of vacancy clusters favourable. The binding energies of such clusters are very high, and the

Simulated properties of U_3O_8			
Property	Experiment	CASCADE	
a	6.812 [90]	6.96	Å
b	6.812 [90]	6.96	Å
c	4.142 [90]	4.13	Å
E_L		-506.474	eV
$\epsilon_{11}^0, \epsilon_{22}^0$		18.465	ϵ_0
ϵ_{33}^0		5.713	ϵ_0
$\epsilon_{11}^\infty, \epsilon_{22}^\infty$		3.769	ϵ_0
ϵ_{33}^∞		3.213	ϵ_0
$\langle \epsilon^0 \rangle$		13.222	ϵ_0
$\langle \epsilon^\infty \rangle$	3.73 [112]	3.577	ϵ_0
E_F		7.333 (3.667)	eV
E_S		62.529 (5.684)	eV

Table 5.16: U_3O_8 crystal properties reproduced by “CASCADE”. The Frenkel and Schottky energies between Brackets have been normalised to an energy per defect.

Defect	Stoichiometry	
	U_3O_{8-z}	U_3O_8
$V_O^{\bullet\bullet}$	0.00	3.67
O_i''	7.33	3.67
$V_U^{-5\frac{1}{3}}$	20.87	11.10
$V_{UO}^{-3\frac{1}{3}}$	15.47	9.36
$V_{UO_2}^{-1\frac{1}{3}}$	10.98	4.84
$V_{UO_3}^{\frac{2}{3}}$	6.32	2.65

Table 5.17: The effective equilibrium formation enthalpies of intrinsic defects in U_3O_8 and U_3O_{8-z} . All energies are reported in [eV].

equilibrium formation enthalpies of $V_{UO}^{-3\frac{1}{3}}$ and $V_{UO_2}^{-1\frac{1}{3}}$ (Table 5.17) are low compared to the formation of $V_U^{-5\frac{1}{3}}$. Nevertheless formation energies of uranium vacancies are always high. Therefore we cannot at present explain the very low uranium migration enthalpy of 2.3 eV measured by Glasser-Leme and Matzke [48] in terms of a mechanism that requires the formation of a uranium vacancy.

It is possible that the predicted formation enthalpy of $V_U^{-5\frac{1}{3}}$ defects decreases if a different model is used in our simulations. At present a uranium ion charge of $5\frac{1}{3}$ is used, perhaps local charge redistribution lowers the migration enthalpy and enhances the formation of cation vacancies or vacancy clusters in the real material.

5.3.4 Intrinsic defect mobility in U_3O_8

Oxygen migration

Because U_3O_8 exhibits a more complex structure (see Figure 5.15) than UO_2 , it is not possible to determine the oxygen migration pathway by inspection of the crystal

lattice symmetry. However, since U_3O_8 is a layered structure we can begin by assuming that migrating species remain in the basal plane. Four different vacancy assisted oxygen migration pathways can then be identified, and Figures 5.16, 5.17, 5.18 and 5.19 show, for each step, the contour plots for the defect energy as a function of migrating oxygen ion position.

The migration activation enthalpies for oxygen in U_3O_{8-z} derived from Figures 5.16, 5.17, 5.18 and 5.19 are all essentially the same: 0.25 ± 0.05 eV.

Since the Frenkel energy is 3.66 eV, the predicted oxygen migration enthalpy in stoichiometric U_3O_8 is 3.9 eV, but in U_3O_{8-z} it will only be 0.25 eV.

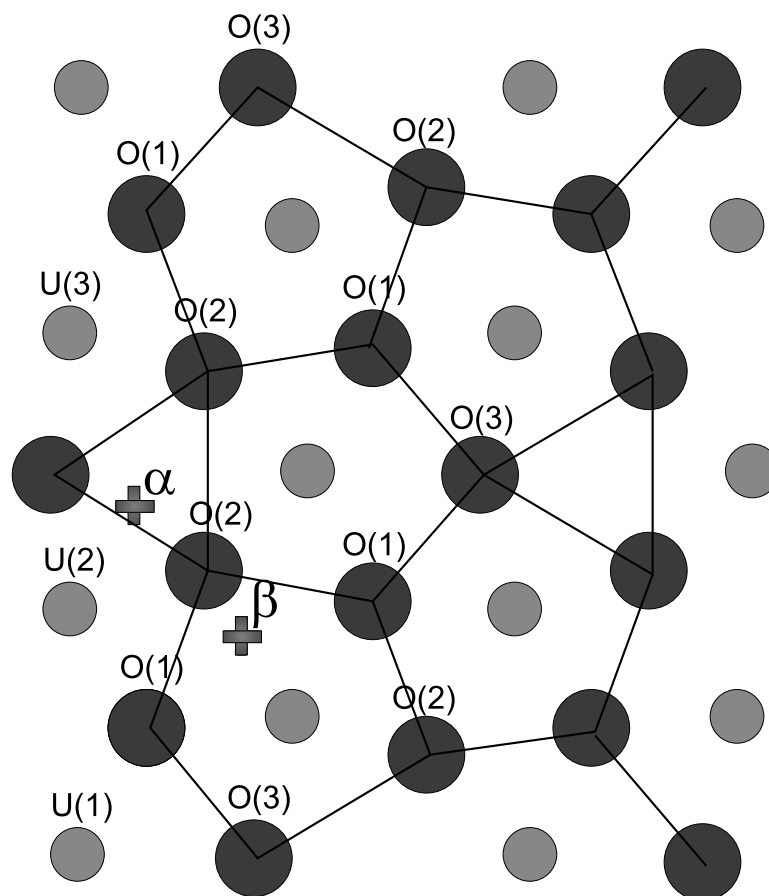


Figure 5.15: The [001] plane of the U_3O_8 structure. α and β are the interstitial positions above and below the shown crystal plane. OX (chain) type oxygen ions exist in the interstitial layer between the uranium ions.

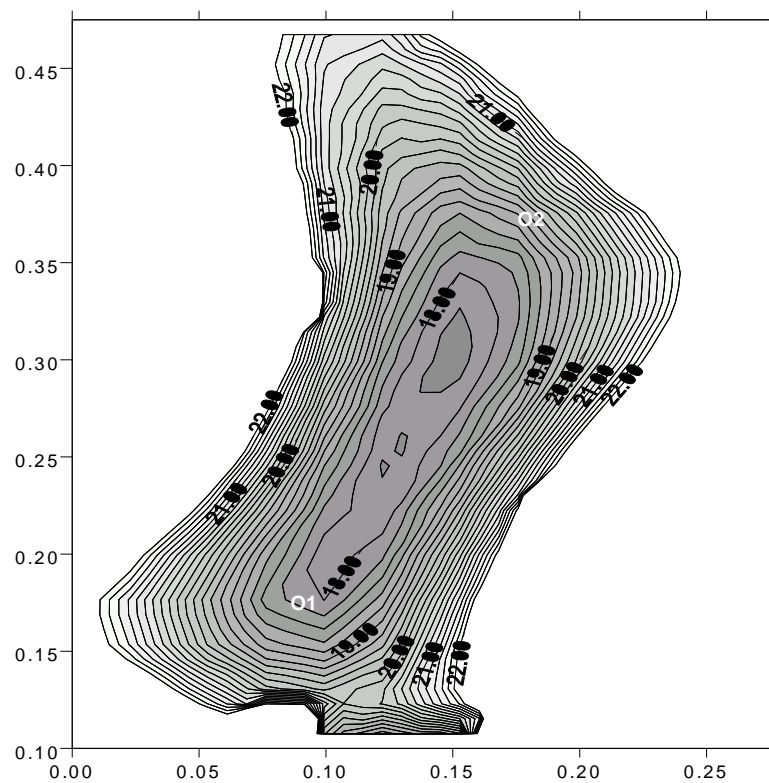


Figure 5.16: Contour plot of migration profile for an oxygen ion in a $O(1):O(2)$ vacancy.

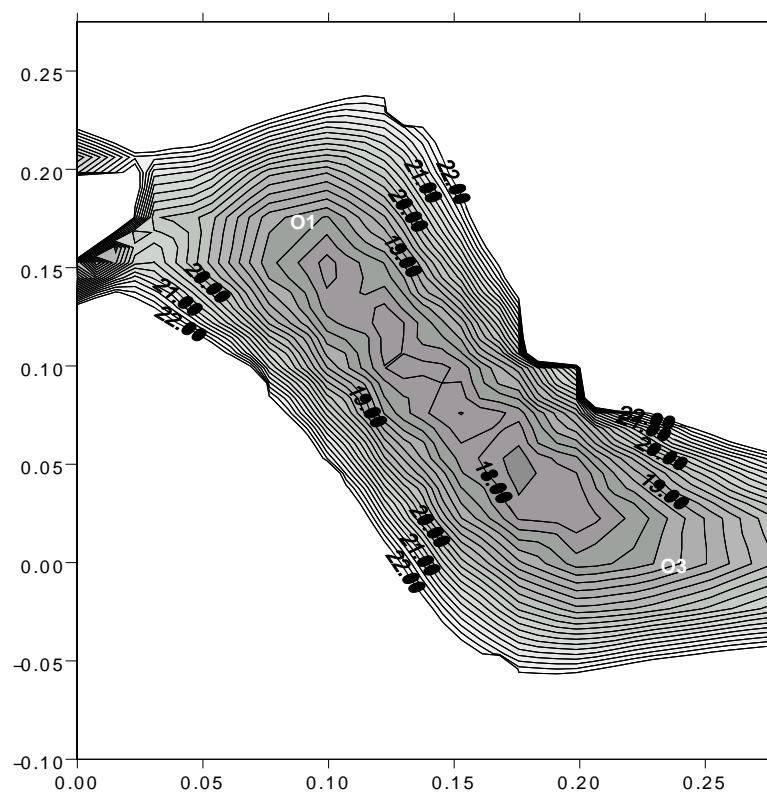


Figure 5.17: Contour plot of migration profile for an oxygen ion in a $O(1):O(3)$ vacancy.

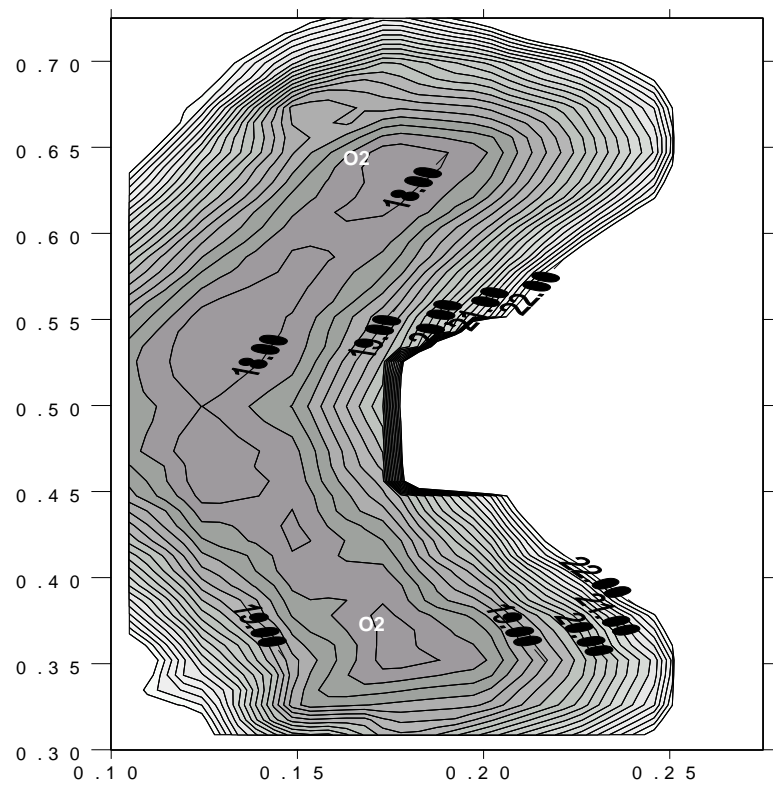


Figure 5.18: Contour plot of migration profile for an oxygen ion in a $O(2):O(2)$ vacancy.

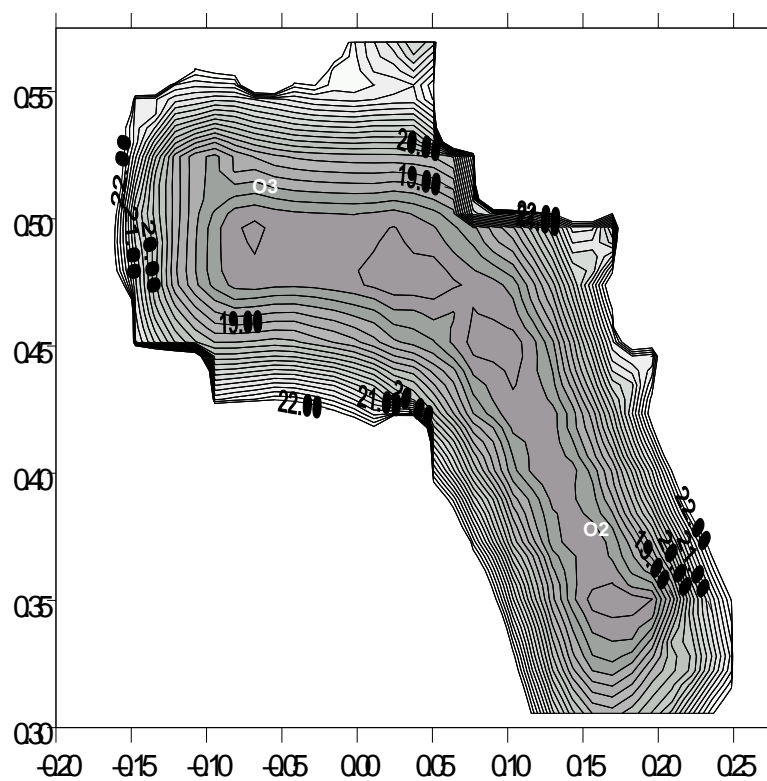


Figure 5.19: Contour plot of migration profile for an oxygen ion in a $O(2):O(3)$ vacancy.

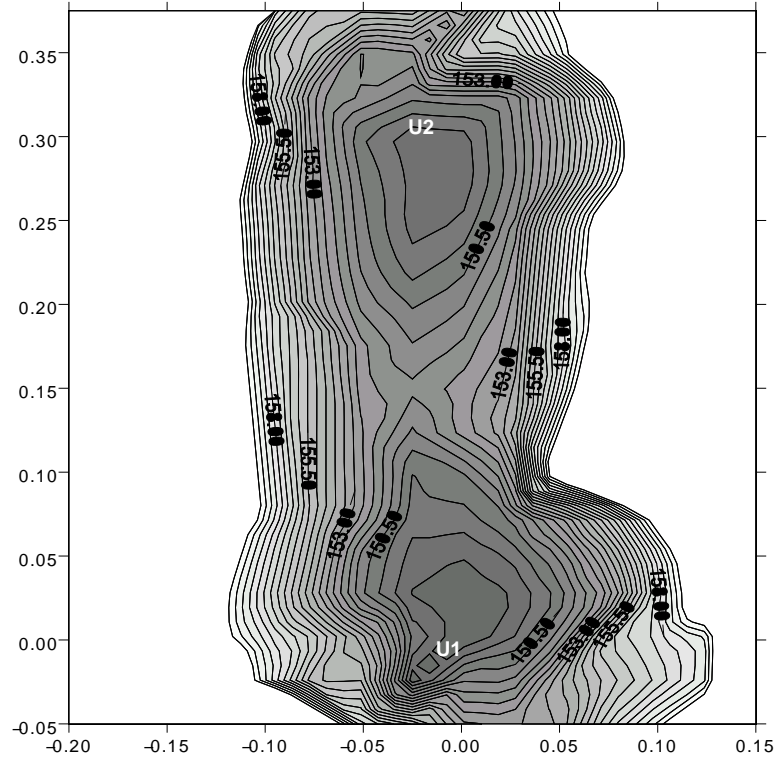


Figure 5.20: This contour map shows the defect energy of a uranium ion as a function of its position on a plane between the U(1) and U(2) lattice sites in U_3O_8 .

Uranium migration

The symmetry in U_3O_8 is such that all uranium migration steps within the basal plane are equivalent. Figure 5.20 shows a total energy contour plot of a uranium ion moving between two uranium sites U(1) and U(2)

The migration enthalpy of a uranium ion is approximately 2.5 eV, which is low compared with the results for UO_2 . However, the formation of uranium vacancies is energetically very expensive and would yield a migration enthalpy of more than 23 eV in U_3O_{8-z} and 13.6 eV in U_3O_8 .

The calculations presented here do not seem to be able to provide the complete

story and further work should include the investigation of alternative potentials that can reproduce the structure equally well as the present set *and* are able to model the charge transfers that must take place when a uranium vacancy is created.

5.4 Fission products in U_3O_8

5.4.1 Solution of Cs_2O in U_3O_8

A large number of complex defects may possibly accommodate large ions such as caesium (radius 1.67 Å) and iodine (radius 2.20 Å). Table 5.18 shows all defect geometries considered and reports the binding energies for caesium inclusion. In this case, the binding energy is defined to be the difference between the empty trap site formation energy and the energy of the caesium filled trap site.

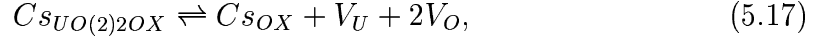
Clearly the binding energy is largely Coulombic in nature, and hence defects with a small negative charge preferentially accommodate the Cs^+ ion. Table 5.18 does not take into account the formation of the accomodating defect or the dissociation of the source of caesium ions.

When considering solution relative to Cs_2O , the picture changes. Table 5.19 shows the equilibrium solution enthalpies for solution of Cs_2O in U_3O_8 and U_3O_{8-z} . Regardless of the fact that the binding energy to oxygen vacancies is unfavourable, the sheer abundance of oxygen vacancies in hypo-stoichiometric U_3O_{8-z} reduces the solution enthalpy of caesium in an OX type vacancy significantly. The Cs_{OX} defect is not the equilibrium solution site since the α site provides a lower energy, but it will play a role in migration mechanisms.

In stoichiometric U_3O_8 caesium prefers to occupy a V_{UO_3} type vacancy. V_{UO_2} and V_{UO} type vacancies have a slightly higher solution enthalpy.

5.4.2 Migration of caesium in U_3O_{8-z}

In U_3O_{8-z} two caesium accomodating defects react in the following way to allow migration of caesium:



where $Cs_{UO(2)2OX}$ is a caesium filled tetra-vacancy cluster consisting of one cation and three anion vacancies.

Effectively a V_{UO_3} accomodating a caesium ion dissociates into a caesium filled chain oxygen vacancy and one uranium and two oxygen planar vacancies.

A possibility, not studied in this thesis, is that the uranium and oxygen vacancies bind and diffuse together. The formation of such a defect is certainly favourable although the dynamics of the diffusion of such a cluster are, as of yet, unknown.

The $Cs_{UO(2)2OX}$ defect initially seemed to be a large defect cluster, where the impurity ion sits in the middle (β -position in Figure 5.21). This was in fact an artifact of the symmetry restriction used in CASCADE, and when the simulation symmetry was broken, the caesium ion relaxed to an out of plane site, showing again the danger of using symmetry restrictions. The caesium impurity can occupy two symmetric positions, indicated by α 's in Figure 5.21. The original symmetric position is the saddle point for internal migration of caesium in the trap. The migration energy in this trap is the difference between the defect energies of the α and β sites : 0.13 eV. The total Arrhenius energy is 2.39 eV, which is about the same as the uranium self diffusion which is therefore the controlling factor since the migration mechanism relies on uranium vacancy migration.

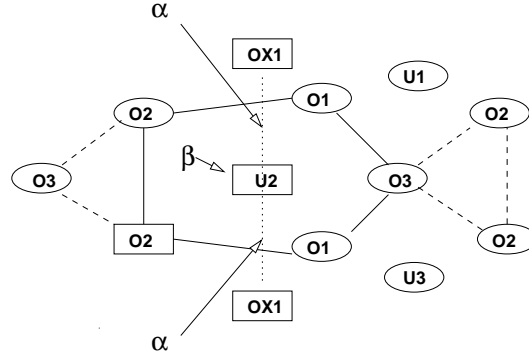


Figure 5.21: Two sites in the halter-shaped $V_{U(1)O(2)2OX(1)}$ defect. Caesium was thought to go in the symmetric β -position, but when symmetry was removed, it was apparent that two symmetric positions near the vacant OX(1) positions are more likely sites.

5.4.3 Migration of caesium in U_3O_8

In stoichiometric U_3O_8 caesium occupies a $Cs_{U(1)O(2)OX(1)}$ defect. Here oxygen vacancies are not as readily available as in U_3O_{8-z} , and a mechanism depending on caesium trapped at a single oxygen vacancy would cost 5.18 eV for migration in the z-direction via OX(1) and 9.01 eV for planar migration via O(1) and O(2) vacancies.

The association of a uranium vacancy with a migration cluster is an alternative migration method. Table 5.19 shows two Cs_{U_2O} and a $Cs_{U_2O_2}$ defect that may assist the migration of caesium in U_3O_8 . In particular the $Cs_{U(1)O(1)O(2)U(2)}$ trap would result in a migration energy of 2.28 eV.

Due to computational constraints all $V_{U_2O_2}$ defects could not be simulated and a complete picture of the migration options is therefore not yet available. The configuration of the defect becomes increasingly difficult and processor time increases with defect complexity. In addition one needs to be wary of symmetry and convergence problems. Similar to the mechanism involving the Cs_{OX} intermediary trap

site, a mechanism employing $V_{U_2O_2}$ type trap sites is expected to show some degree of anisotropy.

Comparing migration behaviour in $UO_{2\pm x}$, the trend of reduced Arrhenius energy for diffusion with increased oxygen content is also predicted to occur in the higher oxide U_3O_8 . In fact, the transformation of UO_{2+x} into U_3O_{8-z} is accompanied by a reduction in the migration energy and then again, albeit less so, when stoichiometry is increased to U_3O_8 .

A summary of the derivation of the caesium migration enthalpy in both the hypo-stoichiometric and the stoichiometric material is shown in Table 5.20. Thus as oxidation proceeds we would expect this to be associated with a gradual increase in the rate of caesium release.

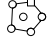








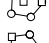






Calculated caesium filled cluster formation energies in U_3O_8			
Defect		Formation E. [eV]	Binding E. [eV]
Anion Vacancies			
O(1)		23.265	-6.782
OX(1)		19.434	-2.951
Cation Vacancies			
U(1)		138.836	6.877
Di-vacancies			
OX(1)OX(2)		37.814	-4.848
U(1)O(1)		150.687	11.509
U(1)O(2)		150.095	12.101
U(1)O(3)		152.856	9.340
U(1)OX(1)		149.130	13.066
Tri-vacancies			
U(1)O(1)O(1)		163.534	15.145
U(1)O(1)O(2)		164.321	14.358
U(1)O(1)O(2)		162.345	16.334
U(1)O(1)O(3)		165.531	13.148
U(1)O(2)O(2)		162.36	16.319
U(1)O(2)O(3)		164.726	13.953
U(1)O(1)OX(1)		162.040	16.639
U(1)O(2)OX(1)		161.719	16.960
U(1)O(3)OX(1)		163.674	15.005
U(1)OX(1)OX(1)		161.875	16.804
Tetra-vacancies			
U(1)O(1)O(1)O(2)		177.717	17.445
U(1)O(1)O(1)O(3)		180.801	14.361
U(1)O(1)O(2)O(3)		181.063	14.099
α -U(1)O(2)OX(1)OX(1)		175.111	20.051
β -U(1)O(2)OX(1)OX(1)		175.243	19.919
U(1)U(1)OX(1)		290.010	17.899
U(1)U(2)O(1)		296.625	11.284
U(1)U(2)O(2)		296.805	11.104
U(1)U(3)O(1)		295.590	12.319
U(1)U(3)O(3)		298.012	9.897
U(1)U(2)O(1)O(2)		309.191	15.201

Table 5.18: Calculated caesium filled defect energies. The binding energy is the energy gained by clustering the caesium ion and the individual vacancies making up the defect. The small pictures represent the geometry of the clusters.

Caesium filled defects in U_3O_8		
Energies are in eV		
Defect	U_3O_{8-z}	U_3O_8
$Cs_{O(1)}$	9.16	14.66
Cs_{OX}	<u>5.33</u>	10.83
Cs_{OX_2}	7.23	15.73
Cs_U	16.34	8.40
Cs_{UOX}	10.16	5.88
$Cs_{UO(2)OX}$	6.26	<u>5.65</u>
$Cs_{U(1)O(2)OX(1)OX(1)}$	<u>3.17</u>	6.23
$Cs_{U(1)O(1)U(2)}$	25.90	11.85
$Cs_{U(1)OX(1)U(1)}$	26.17	12.11
$Cs_{U(1)O(1)O(2)U(2)}$	21.99	7.93

Table 5.19: Equilibrium solution energies of Cs_2O in U_3O_8 . Energies of significance to solution or migration are underlined.

Construction of the predicted Arrhenius energies.				
	U_3O_{8-z}		U_3O_8	
Equilibrium solution trap and energy	$CS_{U(1)O(2)2OX(1)}$	3.17	$CS_{U(1)O(2)OX(1)}$	5.65
Most likely assisting trap and solution energy	$CS_{OX(1)}$	5.33	$CS_{U(1)O(1)O(2)U(1)}$	7.93
Migration energy	0.13		n/a	
Total energy of process:	2.39		2.28	
Self diffusion of uranium:	2.4		2.4	
Final predicted activation energy:	2.4		2.4	

Table 5.20: The predicted Arrhenius activation energies for caesium migration. Predictions are constructed from the trap formation, the self diffusion of cations in the lattice and the internal migration of the ions in the migration assisting traps. The self diffusion activation energy of uranium is not known with great certainty. Here the value observed by Glasser-Leme [48] is used as an indication for both U_3O_{8-z} and U_3O_8 .

5.4.4 Solution of iodine in U_3O_8

Calculations were performed on the solution of iodine in α - U_3O_8 for the available charge states of the fission product. Because the number of simulations performed is so much larger than for the caesium ions above, the data is summarized and the raw defect calculation results are omitted.

The electric field at some oxygen vacancy sites is strong enough to displace the applied iodine shell far enough to disrupt the relaxation calculation. By adding a third order term to the core-shell interaction, the shell can be forced to remain with the core. Subsequent restarting of the calculations from the relaxed situation with a reduced third order term and repeating this process eventually results in a fully converged defect energy without an anharmonic term in the core-shell interaction.

The solution enthalpies of iodine in U_3O_{8-z} are listed in Table 5.21. Although it was not possible to execute all defect calculations it is clear that iodine prefers the I^- charge state. Furthermore, vacancy clusters consisting of two oxygen vacancies are the preferred solution sites.

In stoichiometric U_3O_8 (see Table 5.22) iodine prefers a O(3) type oxygen vacancy although interstitial solution is only 0.8 eV less favourable. Interestingly the O(1) and O(2) type vacancies show much higher solution enthalpies than the O(3) type.

5.4.5 Migration of iodine in U_3O_8

We have studied the behaviour of interstitial iodine, moving parallel to the basal plane through the layer of the so called chain oxygen ions. Figure 5.22 shows a plot of the energy of an interstitial ion at different positions in the lattice. The area of the crystal covered by this energy contour plot is the area where the two interstitial positions are indicated in Figure 5.15. The activation energy for interstitial

Solution energy of Iodine in U_3O_{8-z}				
Defect	I^-	I	I^+	I^{2+}
Interstitials				
α -site	2.036	7.989	12.366	15.137
β -site	2.180	11.35	16.232	
Oxygen substitutional defects				
O(1)	1.175	9.409	17.081	
O(2)	-2.446		14.906	
O(3)	0.874		15.021	
OX(1)		8.6	15.74	
Uranium substitutional defects				
U(1)			28.77	23.40
Oxygen di-vacancies				
O(1)O(2)	-2.414			
O(1)O(3)	-1.37			
O(2)O(2)	-3.609			
O(2)O(3)	-3.608			
OX(1)O(1)	-3.285			
OX(1)O(2)	-4.129			
OX(1)O(3)	-4.413			
O(1)xO(1)	-0.743			
O(2)xO(2)	-0.197			
O(3)xO(3)	-2.197			

Table 5.21: Solution energies are calculated relative to a hypothetical free neutral iodine ion. O(n)xO(n) indicates a di-vacancy trap where vacancies are not located in the same basal plane.

Solution energy of Iodine in U_3O_8				
Defect	I^-	I	I^+	I^{2+}
Interstitials				
α -site	2.04	7.99	12.37	15.14
β -site	2.18	11.35	16.232	
Oxygen substitutional defects				
O(1)	5.07	13.08	20.75	
O(2)	5.74		18.57	
O(3)	1.22			
OX(1)		12.36	19.40	
Uranium substitutional defects				
U(1)			18.99	13.62

Table 5.22: Solution energies are calculated relative to a hypothetical free neutral iodine ion. Larger oxygen di-vacancies are not reported here as their formation enthalpies are much higher than in U_3O_{8-z} and play no part in stoichiometric U_3O_8 .

migration in the chain oxygen layer is approximately 2.6 eV.

Since the interstitial position is not the equilibrium solution site for iodine in the stoichiometric oxide, we need to add 0.8 eV (i.e. 2.04-1.22 eV, see Table 5.21) to get the Arrhenius energy prediction for the total process.

However, the equilibrium solution site in U_3O_{8-z} is more likely to be an oxygen di-vacancy, which suggests a oxygen vacancy assisted diffusion mechanism. The interstitial mechanism remains the most likely mechanism for the stoichiometric phase, because the availability of oxygen vacancies is reduced drastically in stoichiometric U_3O_8 . There are some large vacancy clusters (V_{UO_2} and V_{UO_3}) with reasonably low solution energies, but at present no mechanism is obvious for migration by way of those clusters.

5.4.6 Vacancy assisted migration in U_3O_{8-z}

Since the equilibrium solution site for iodine seems to be the oxygen di-vacancy, iodine can migrate via two different mechanisms, both of which are considered here:

- The loss of a vacancy followed by the “docking” of a new vacancy somewhere onto the defect and internal re-arrangements in the defect.
- The acquisition of a vacancy followed by an internal migration step and the loss of a different vacancy.

If we assume that internal migration and the association/dissociation of a vacancy are simple activated processes with low activation energies, we may predict a lower limit for the migration enthalpy. This is equal to the reaction energy of the association/dissociation processes required to provide mechanisms that transport iodine through the unit cell. The reaction energy is equal to the difference in

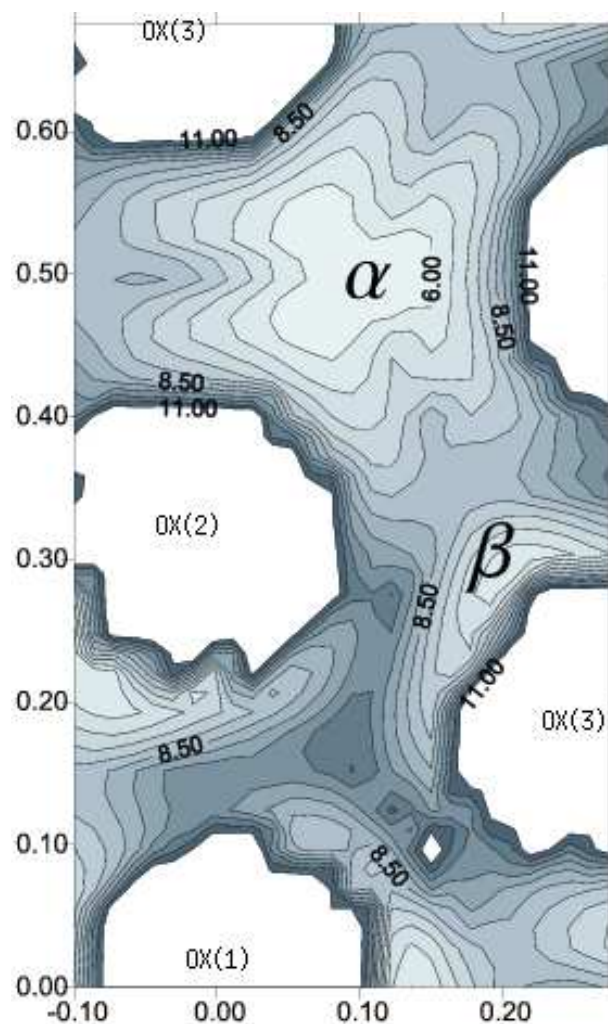


Figure 5.22: A contour plot of the energy of an interstitial iodine ion moved through the lattice. The migration energy barrier between interstitial site α to site β is approximately 2.6 eV.

solution energies at different sites.

Figure 5.23 shows the possible steps an iodine ion needs to make in order to migrate in the basal plane. The figure clearly indicates that iodine ions prefer to be adjacent to the O(2) and O(3) oxygen positions. A migration mechanism along the basal plane would yield an activation energy of approximately 2.2 eV.

The solution energy of a cross plane O(3)xO(3) trap is only 1.6 eV more than the equilibrium solution site in a O(2)O(2) or O(2)O(3) vacancy. If we ignore the activation energy for the reaction path, we end up with an activation energy of 1.6 eV for migration through U_3O_{8-z} along the z-axis of the crystal structure.

Based on this level of approximation it seems the iodine migration is unlikely to be highly anisotropic despite the hexagonal crystal structure of α - U_3O_8 .

5.4.7 Solution of ruthenium in U_3O_8

Fission products with a positive charge state which are small relative to oxygen are expected to occupy solution sites such as the cation substitutional, interstitial or small complexes, for example, $\{V_U : V_O\}^{-3\frac{1}{3}}$. In U_3O_8 the issue of preferred site is further complicated by the existence of 4 crystallographically different anion sites, 3 cation sites and 2 interstitial sites. Fortunately, it has been demonstrated that practically the cation sites are energetically equivalent [114,115].

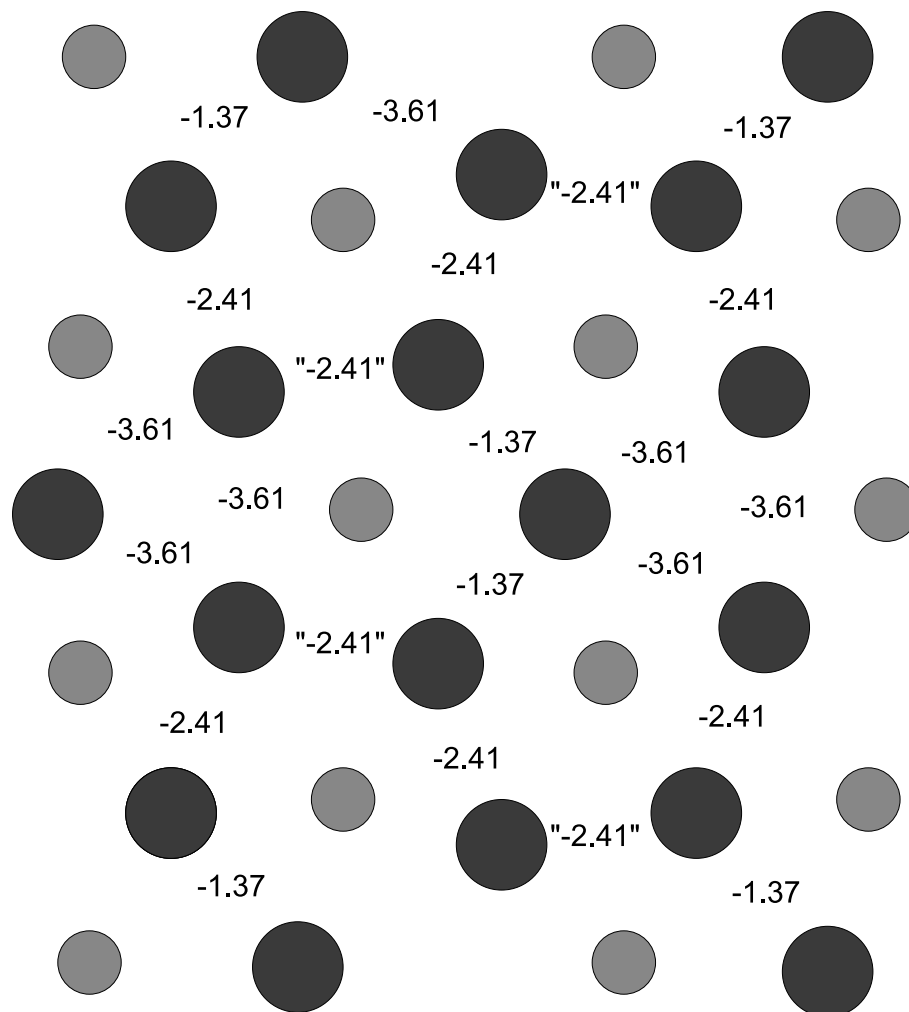
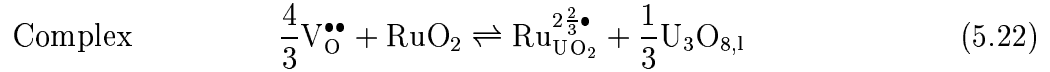
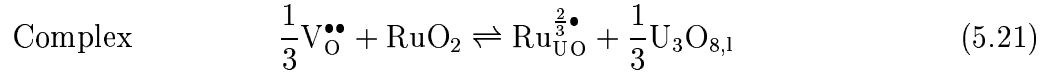
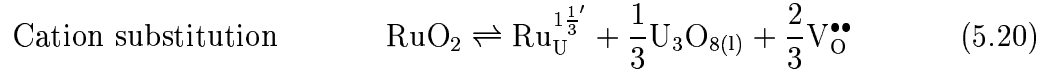


Figure 5.23: The figure shows the energy for solution of iodine when it is associated with $V_O : I_i : V_O$ type clusters. The text roughly indicates the positions of the iodine atoms between two vacant oxygen positions.

Likely solution reactions are:



In these reactions we assume a Ru^{4+} charge state. If we wish to evaluate other charge states the solution energy of that charge state needs to be calculated specifically and the ionization energies included as described previously for UO_2 in Section 5.2.2. Since, according to Wittingham [83] further oxidation of RuO_2 to RuO_3 and RuO_4 only occurs at the surface, we do not consider the higher charge states associated with those oxides.

U_3O_{8-z} The predicted solution enthalpies for RuO_2 in hypostoichiometric U_3O_{8-z} are listed in Table 5.23. Within the uncertainties of these calculations, we predict the equilibrium charge state and solution site to be Ru^+ or Ru^{2+} in the α -interstitial position. The low charge state is a consequence of two factors; the favoured site being an interstitial site and the relatively high ionization energies of ruthenium compared to uranium. The interstitial site is favoured because, in U_3O_{8-z} , the high oxygen vacancy concentration reduces the uranium vacancy concentration to practically zero through the Schottky equilibrium.

The solution enthalpy values in Table 5.23 also demonstrate quite clearly that RuO_2 is highly soluble in U_3O_{8-z} . It is possible that these low charge state interstitial ions may aggregate and reduce further to form metal inclusions as they do

Ion:	U_3O_{8-z}					U_3O_8				
	Ru	Ru ⁺	Ru ²⁺	Ru ³⁺	Ru ⁴⁺	Ru	Ru ⁺	Ru ²⁺	Ru ³⁺	Ru ⁴⁺
Interstitial:										
α	-5.40	<u>-10.21</u>	<u>-9.67</u>	-5.87	-	9.94	3.13	<u>1.66</u>	3.47	-
β	-1.68	-6.70	-6.26	-3.13	1.14	13.66	6.64	5.07	6.20	8.48
Oxygen Vacancy:										
O(1)	-1.57	-2.98	-0.56	9.94	19.83	17.43	14.02	14.44	22.94	30.83
O(2)	-2.80	-4.47	-1.57	2.99	8.28	16.20	12.53	13.43	16.00	19.28
O(3)	-2.80	-4.47	-1.57	2.99	8.28	16.20	12.53	13.43	16.00	19.28
OX(1)	-	-7.23	-5.30	-0.58	8.86	19.00	9.77	9.70	12.42	19.86
Uranium vacancy:										
U(1)	9.47	2.82	-0.76	-0.33	4.67	15.02	6.38	<u>0.80</u>	<u>-0.77</u>	2.23
Complex trap:										
UO(1)	5.57	-1.47	-3.96	-2.46	2.98	14.79	5.75	<u>1.26</u>	0.76	4.21
UO(2)	4.67	-1.85	-3.88	-2.38	3.28	13.90	5.37	<u>1.35</u>	0.85	4.50
UO(3)	6.21	0.11	-2.83	-1.72	-	15.44	7.33	2.39	1.50	-
UOX(1)	4.03	-2.10	-3.86	-1.78	3.84	13.26	5.12	<u>1.36</u>	1.44	5.06

Table 5.23: The solution energies (eV) for ruthenium ions in U_3O_{8-z} and U_3O_8 . In the evaluation of the solution mechanisms we assume an electron affinity of 0 eV for U_3O_{8-z} and an affinity of 2 eV for U_3O_8 (see text).

in UO_2 . However, this seems unlikely since the solution energy associated with Ru^0 is much less negative than that associated with Ru^+ . Furthermore, in UO_2 and UO_{2-x} where metal particles are known to form readily, the Ru^0 solution charge state was preferred over Ru^+ . Nevertheless, it would be worthwhile investigating this possibility further to definitely rule it out.

U_3O_8 In stoichiometric U_3O_8 , the situation changes. The equilibrium charge state and solution site predicted in Table 5.23 is Ru^{3+} at a cation vacancy. Alternative solution sites and charge states are interstitial Ru^{2+} , cation substitutional Ru^{3+} and Ru^{2+} in $V_{UO(1)}$ and $V_{UO(2)}$ trap sites, but these are significantly less stable.

The uranium vacancy is, of course, now a logical solution site since uranium vacancies can be more easily formed in U_3O_8 compared to U_3O_{8-z} . In such a highly charged site, there is then sufficient Madelung potential to stabilize a higher charge state of the ruthenium ion. Nevertheless, ruthenium still does not ionize to Ru^{4+} . A similar result has been observed in a study of molybdenum in $UO_{2\pm x}$ [108] where Mo^{4+} was not predicted to be as stable as Mo^{3+} and of course for ruthenium in $UO_{2\pm x}$ (see Section 5.2.4).

Although the solution energy in U_3O_8 is predicted to be negative (i.e. ruthenium is soluble), the uncertainties in these calculations, particularly in the ionization energy of the lattice, make this conclusion less strong than the same conclusion in U_3O_{8-z} . What is much more clear, however, is that if RuO_2 is soluble, the solution mechanism must include a step where the Ru valence state is lowered to Ru^{3+} . Furthermore, ruthenium is certainly less soluble in U_3O_8 than it is in U_3O_{8-z} .

5.4.8 Migration of ruthenium in U_3O_8

U_3O_{8-z} Since the equilibrium solution site has such a low enthalpy compared to all alternative trap sites, it seems sensible to consider only interstitial migration. Figures 5.24 and 5.25 show a contour plot of the defect energy of ruthenium as it migrates perpendicular to the c axis between the layers of the structure. The migration energy of Ru^+ in the U_3O_8 structure is 4.5 ± 0.5 eV. (The inaccuracy of 0.5 eV is a result of the difficulty in tracing a migration path over a grid of calculation results with a mathematical method and the quantization error of reading it from a contour plot.) If we assume that Ru^{2+} is the equilibrium charge-state, the migration energy is 4.0 ± 0.5 .

U_3O_8 Unlike the U_3O_{8-z} case above, in stoichiometric U_3O_8 alternative solution sites are possible. A complex migration pathway from ruthenium trapped at a cation vacancy to the capture of an oxygen and yet another cation vacancy followed by an internal migration step of the ruthenium in the trap is possible (compare with, for example, caesium migration in U_3O_8).

Alternatively, ruthenium might de-trap, migrate interstitially and trap at a cation site again. This last mechanism has the advantage that it does not rely on cation migration. Also the migration pathways can be long, as cation vacancy concentrations are low. Effectively this would lead to an increase in the pre-exponential in the diffusion equation. An interstitial migration mechanism is possible for ions which go into non-equilibrium solution at α -interstitial sites. This mechanism should yield a migration energy of 4.5eV plus 2.43 eV for the non-equilibrium reaction. Regardless of the mechanism, we expect the activation energy for ruthenium migration in stoichiometric U_3O_8 to be significantly higher than in U_3O_{8-z} .

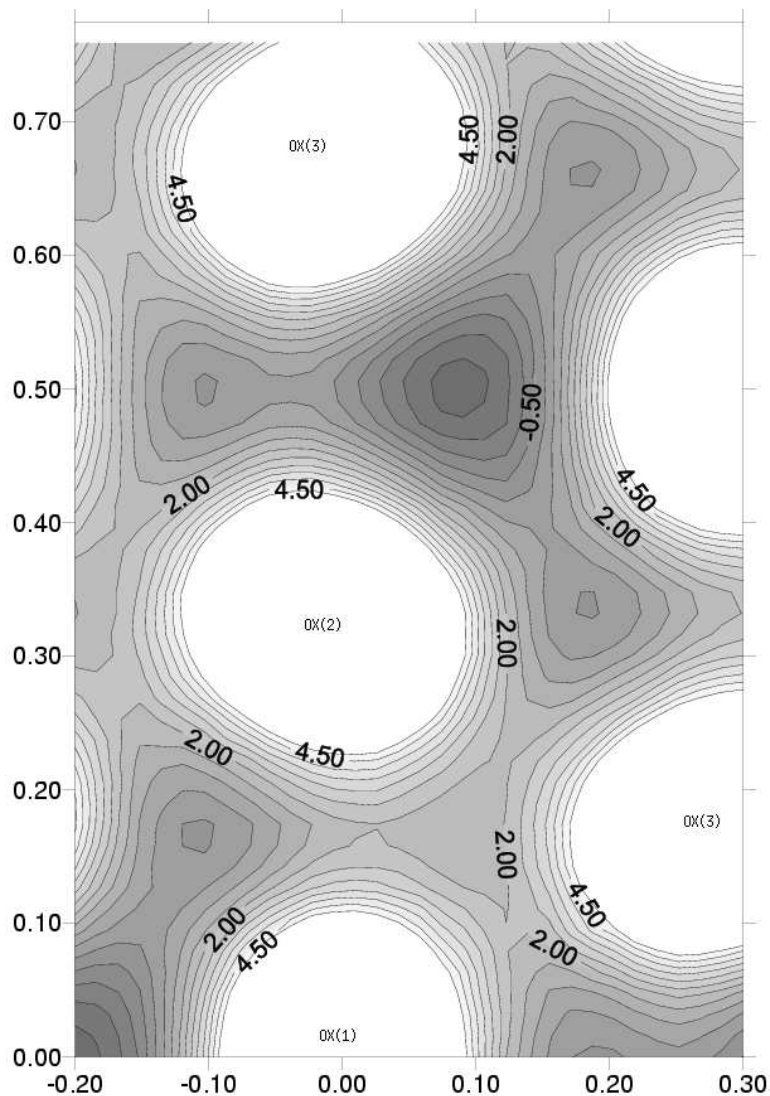


Figure 5.24: Contour plot of the defect energy of a Ru^+ interstitial ion in different positions in the U_3O_8 structure. Ruthenium ions will prefer to sit in the dark areas and migrate around the white areas (where the Coulombic interaction with uranium cations is strongly repulsive). The migration energy is 4.5 ± 0.5 eV.

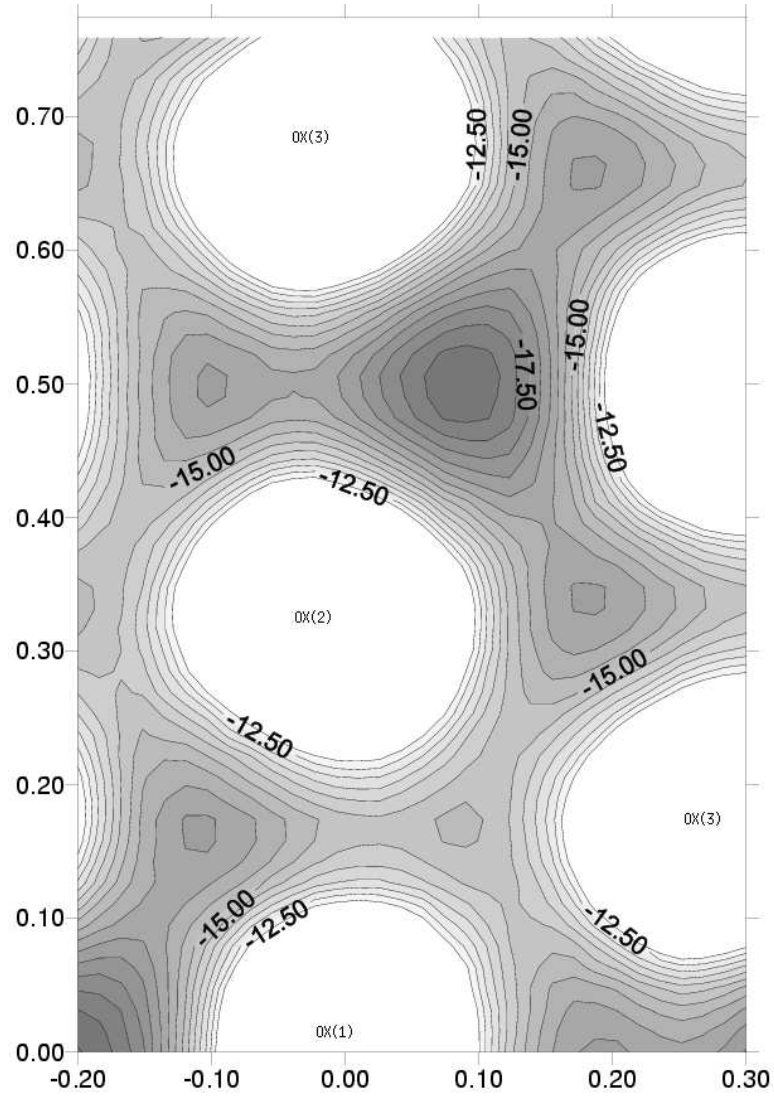


Figure 5.25: Contour plot of the defect energy of a Ru^{2+} interstitial ion in different positions in the U_3O_8 structure. The migration energy is 4.0 ± 0.5 eV.